The Quantum-Geometric Correspondence: Axioms, Gravitational Decoherence, and the Wheeler–DeWitt Rate

Quantum-Geometric Correspondence

Marc Sperzel*

Independent Researcher
MSci Physics, King's College London

Abstract

We present the canonical formulation of the Quantum-Geometric Correspondence: the hypothesis that quantum mechanics and general relativity are complementary projections of a single underlying reality. The framework rests on three primitive axioms—Generalized Entropy Conservation (unifying the conservation of total quantum information with the entanglement–area correspondence), the Entropic Action Principle, and Scale-Dependent Unification—from which we derive an observer-dependent horizon principle, a holographic information bound, and the Semiclassical Duality Correspondence: in the semiclassical regime a matter superposition becomes entangled with a superposition of gravitational field configurations. Tracing over the inaccessible geometry then yields gravitational decoherence, the framework's sharpest laboratory prediction. Its energy scale is the gravitational self-energy $E_{\mathrm{G}} = GM^2/d$, giving $\tau_{\mathrm{dec}} = \hbar d/(GM^2) \approx 1.6$ ns for a 1 μg particle separated by 1 mm. We show that the standard product initial state used in perturbative quantum field theory (which predicts a G^2 rate and $\tau_{\mathrm{dec}} \sim 10^{18}$ yr) violates the linearized Wheeler–DeWitt constraint; imposing the constraint forces an entangled initial state and replaces the noise-kernel mechanism with a coherent-state-overlap mechanism, yielding G^1 scaling, with the central operator identity $K = 2\pi H_{\mathrm{phys}} + \mathcal{O}(G^2)$. The Margolus–Levitin quantum speed limit bounds the rate coefficient to $C \in [2/\pi, 1]$ in $\Gamma_{\mathrm{dec}} = C\,E_{\mathrm{G}}/\hbar$, with natural value $C = 1$. The G^1 and G^2 predictions differ by $\sim 3 \times 10^{34}$ at the laboratory benchmark, making the scaling experimentally decidable. The mechanism extends to quantum fields via the stress-energy operator, giving Fock-state rates and a self-gravitational route to the classicalization of inflationary perturbations. The same three axioms underlie the holographic dark energy and emergent-gravity results developed in companion work.

Contents

*ORCID: 0009-0000-6252-3155. Email: me@marcsperzel.com

Part I
Framework

1 Introduction

The reconciliation of quantum mechanics and general relativity remains the central open problem in theoretical physics. Despite nearly a century of effort, no complete theory of quantum gravity has emerged that is both mathematically consistent and empirically verified. String theory, loop quantum gravity, and asymptotic safety each offer partial insights, yet none has produced unambiguous experimental predictions accessible to current technology. The difficulty is not merely technical; it reflects a conceptual tension between the foundational principles of the two theories. Quantum mechanics describes nature in terms of state vectors evolving unitarily in a fixed background spacetime, while general relativity treats spacetime itself as a dynamical entity shaped by matter and energy. Any attempt at unification must address this asymmetry.

In recent years, developments in black hole physics and holography have suggested a possible resolution. The Bekenstein–Hawking entropy formula [1, 2], the Ryu–Takayanagi prescription [3], and the ER=EPR conjecture [4] all point toward a deep connection between quantum entanglement and the geometry of spacetime. These results, emerging from the study of black holes and the AdS/CFT correspondence, suggest that entanglement may not merely correlate distant quantum systems but may actually constitute the fabric of spacetime itself. If this perspective is correct, then quantum mechanics and general relativity are not competing descriptions requiring reconciliation, but complementary projections of a single underlying reality—much as wave and particle descriptions complement one another in ordinary quantum mechanics. We call this perspective the *Quantum-Geometric Correspondence*.

The arc of this paper. This paper develops the Quantum-Geometric Correspondence from first principles and follows a single physical through-line from its axioms to a concrete, falsifiable laboratory prediction. The narrative has four movements.

(i) Axioms (Part I). We build the framework on three primitive axioms: Generalized Entropy Conservation, which unifies the conservation of total quantum information with the identification of entanglement and geometric area; the Entropic Action Principle, which governs the dynamics of coupled matter–geometry systems; and Scale-Dependent Unification, which describes how quantum and geometric descriptions interpolate with scale. From these we derive—as theorems, not further postulates—an Observer-Dependent Horizon Principle, a Holographic Information Bound, and the Semiclassical Duality Correspondence. The last of these is the physical heart of the framework: *a matter superposition does not source a single classical geometry, but becomes entangled with a superposition of gravitational field configurations.*

(ii) The key prediction: gravitational decoherence (Part II). When an experimenter measures only the matter and traces over the inaccessible geometry, this matter–geometry entanglement manifests as decoherence. The energy scale of the effect is the gravitational self-energy of the superposition, $E_{\mathrm{G}} = GM^2/d$ for a mass M split by a separation d, giving a decoherence time

$$\tau_{\mathrm{dec}} = \frac{\hbar d}{GM^2} = \frac{\hbar}{E_{\mathrm{G}}}. \tag{1}$$

For a 1 μg particle separated by 1 mm, this is $\tau_{\rm dec} \approx 1.6$ ns—fast enough to explain why macroscopic superpositions are never observed, yet within reach of next-generation matter-wave interferometry. This is the Diósi–Penrose energy scale, a hypothesis with strong physical motivation [5, 6].

(iii) Its G^1 rate (Part II). The decisive theoretical question is the power of G. Standard perturbative quantum field theory, applied to an unentangled product initial state, predicts a G^2 rate and decoherence times of order 10^{18} years for laboratory masses—effectively unobservable. We show that this product state *violates the linearized Wheeler–DeWitt constraint*: a mass must carry its own Newtonian field. Imposing the constraint forces an entangled initial state and replaces the noise-kernel mechanism (G^2) with a coherent-state-overlap mechanism (G^1). The central operator identity is $K = 2\pi H_{\rm phys} + \mathcal{O}(G^2)$. The two predictions differ by $\sim 3 \times 10^{34}$ at the benchmark, so even an order-of-magnitude measurement is decisive.

(iv) Its coefficient and its reach (Part II and appendices). The G^1 scaling fixes the rate up to an $\mathcal{O}(1)$ coefficient C in $\Gamma_{\rm dec} = C\, E_{\rm G}/\hbar$. The Margolus–Levitin quantum speed limit bounds this coefficient to $C \in [2/\pi,\, 1]$, with the natural value $C = 1$ (Markovian dephasing, the Diósi master equation) and the floor $C = 2/\pi$ (the orthogonalization limit). Finally, the point-mass formula extends to quantum fields by replacing the mass density with the stress-energy operator, yielding decoherence rates for Fock-state superpositions and an application to inflationary perturbations.

A reader should therefore see one idea unfolding: the axioms entangle matter with geometry; the entanglement decoheres the matter; its energy scale is $E_{\rm G}$; its rate is G^1 once the Hamiltonian constraint is imposed; its coefficient is pinned to a narrow window; and it generalizes from particles to fields.

Status of the claims. We are careful throughout to distinguish what is established from what is motivated. The energy scale $E_{\rm G} = GM^2/d$ is established (it is classical gravitational self-energy). The G^1 scaling is *derived in linearized gravity within a controlled approximation* by imposing the Wheeler–DeWitt constraint; the extraction of a *rate* (linear-in-time decay) from this energy scale invokes the Hamiltonian constraint and the Page–Wootters mechanism for emergent time, and is the less rigorous step. The Diósi–Penrose identification of $E_{\rm G}/\hbar$ with the decoherence rate is a hypothesis with strong physical motivation, not a theorem. Standard perturbative QFT, which gives G^2, is correct for its (unconstrained) initial state; the two calculations answer different physical questions. The matter is ultimately empirical, and the framework makes a definite, falsifiable prediction.

Structure. Part I (Framework). Section 2 states the three primitive axioms and derives the horizon, holographic, and duality results. Section 3 develops the entropic dynamics and the thermodynamic origin of local temperature. Section 4 treats scale-dependent unification, the minimum length, and modified dispersion. Section 5 addresses observer-dependent horizons, the generalized uncertainty principle, and vacuum birefringence. **Part II (Gravitational decoherence).** Section 6 establishes the Diósi–Penrose mechanism and the energy scale $E_{\rm G}$. Section 9 imposes the Wheeler–DeWitt constraint on the Feynman–Vernon influence functional and derives the G^1 versus G^2 resolution. Section 10 extracts the rate, folds in the Margolus–Levitin coefficient bound, and gives the numerical prediction. **Part III.** Section 11 collects the testable predictions of the whole framework; Section 12 discusses connections, limitations, and outlook. The appendices provide the logical-independence proofs, the semiclassical mathematical

framework, self-consistency, the decoherence conventions and G-scaling arguments, the coherent-state overlap computation, the robustness of the $\mathcal{O}(G^2)$ corrections, the information-theoretic (Margolus–Levitin) bound, and the second-quantized field extension.

Series context. This is the canonical core paper of the Quantum-Geometric Correspondence series; it absorbs and unifies the previously separate treatments of the framework, the decoherence mechanism, the Wheeler–DeWitt rate, the information-theoretic bound, and the field-theoretic extension. Companion work applies the same axioms to holographic dark energy, $\rho_{\rm DE} = \alpha c^2 H^2/G$ with $\alpha \approx 0.082$ [7], and to emergent gravity and the MOND acceleration scale $a_0 = cH_0/(2\pi)$; we note these connections in passing (Section 12) but do not develop them here.

2 The Axiom Structure

Any attempt to unify quantum mechanics and general relativity must begin with a clear statement of foundational principles. The history of physics demonstrates that axiomatization reveals the conceptual core of a theory. Maxwell's equations, once axiomatized, made the existence of electromagnetic waves manifest; Einstein's postulates for special relativity exposed the conventional nature of simultaneity. We adopt an axiomatic approach because the tension between quantum mechanics and general relativity is fundamentally conceptual, and conceptual tensions are best addressed by making foundational assumptions explicit.

Following Einstein's dictum that a theory should be "as simple as possible, but no simpler," we reduce the framework to *three primitive axioms*, which cannot be derived from more basic principles within the theory: Generalized Entropy Conservation, the Entropic Action Principle, and Scale-Dependent Unification. From these we obtain a series of derived results—an observer-dependent horizon principle, a holographic information bound, and the Semiclassical Duality Correspondence describing how matter superpositions couple to geometry—each a theorem rather than an independent postulate. A single further hypothesis, the Gravitational Information Axiom, fixes the *rate* of gravitational information transfer; we flag it explicitly as a hypothesis, not a primitive axiom. The logical relationships among these statements are clarified throughout this section, and the independence of the three primitive axioms is established through countermodels in Appendix A.

2.1 Axiom I: Generalized Entropy Conservation

The first axiom addresses the fate of quantum information in gravitational processes and its geometric storage. The black hole information paradox, first articulated by Hawking [8], demonstrated that semiclassical gravity appears to destroy information: a pure quantum state collapsing to form a black hole appears to emerge as thermal Hawking radiation, violating unitarity. Decades of work on the paradox—including the Page curve [9], quantum extremal surfaces [10], and island calculations [11]—have converged on the conclusion that information is preserved, though the mechanism requires physics beyond semiclassical gravity. In parallel, holographic results established *where* that information resides: the Ryu-Takayanagi formula [3] identifies the entanglement entropy of a boundary region with the area of a bulk minimal surface divided by $4\ell_P^2$; quantum extremal surfaces [10] and the ER=EPR conjecture [4] extend the correspondence between entanglement and geometry.

We unify both insights into a single primitive axiom: information is conserved when one accounts for both matter and geometry, and the geometric contribution is the Bekenstein-Hawking area term. The von Neumann entropy of matter and the area of horizons are two facets of one conserved quantity, the generalized entropy.

Axiom 2.1 (Generalized Entropy Conservation)**.** *For a closed quantum-gravitational system bounded by a quantum extremal surface or causal horizon $\mathcal{X}$, the generalized entropy*

$$\boxed{S_{gen}(\mathcal{X}) = \frac{A(\mathcal{X})}{4\ell_P^2} + S_{ext}(\mathcal{X})} \tag{2}$$

is conserved under dynamical evolution, while the Generalized Second Law $\delta S_{gen} \geq 0$ holds for open systems. Here $A(\mathcal{X})$ is the proper area of the surface and $S_{ext}(\mathcal{X}) = -\mathrm{Tr}(\rho \ln \rho)$ is the von Neumann entropy of the quantum fields in the exterior region. Equivalently, for the total state,

$$\boxed{S_{total} = S_{vN}(\rho) + \frac{A(\mathcal{H})}{4\ell_P^2} = const.} \tag{3}$$

This single axiom carries two physical messages. First (information conservation): when matter degrees of freedom become inaccessible—as when matter falls behind a black hole horizon—information is not lost but transferred to geometric degrees of freedom; the sum $S_{\mathrm{vN}} + A/(4\ell_P^2)$ remains constant even as its individual terms change, resolving the information paradox within the framework. Second (entanglement-geometry correspondence): because the geometric term is fixed to the area, a change in entanglement *must* be accompanied by a change in geometry. When a quantum system in superposition becomes entangled with its environment, the corresponding geometric degrees of freedom also change, leading to the gravitational decoherence analyzed in Part II. Subleading corrections ΔS_{corr} (logarithmic in A, higher-curvature) become important in strong-gravity regimes but do not alter the leading structure.

2.2 Axiom II: Entropic Action Principle

The second axiom governs the dynamics of coupled matter-geometry systems. Standard general relativity derives Einstein's equations from the Einstein-Hilbert action by varying with respect to the metric. Quantum field theory derives matter dynamics from a matter action by varying with respect to field configurations. The challenge in quantum gravity is to formulate a unified action governing both.

Our approach incorporates entropy directly into the action principle, following insights from thermodynamic approaches to gravity [12]. The idea is that gravity, like thermodynamics, may emerge from more fundamental microscopic physics through entropic considerations. We include not only the usual matter Hamiltonian and gravitational curvature terms, but also an entropic contribution proportional to the von Neumann entropy.

Axiom 2.2 (Entropic Action Principle)**.** *In the semiclassical regime—where gravity is classical ($g_{\mu\nu}$ a c-number) and matter is quantum (ρ a density operator on the fixed background)—dynamics extremizes:*

$$\boxed{S[\rho, g] = \int d^4x\sqrt{-g}\left[\langle \hat{H}_{matter}\rangle_\rho + \frac{c^4 R}{16\pi G} - \frac{s_{vN}(\rho)}{\beta}\right]} \tag{4}$$

where $\langle \hat{H}_{matter} \rangle_\rho = Tr(\rho \hat{H}_{matter})$ *is the matter Hamiltonian density,* $s_{vN}(\rho)$ *is the von Neumann entropy density (entropy per unit volume), and the local inverse temperature* $\beta(x)$ *satisfies the Tolman-Ehrenfest relation* $\beta\sqrt{g_{00}} = const$ *along timelike curves.*

The three terms in this action have clear physical interpretations. The first term is the matter Hamiltonian density, representing matter energy per unit volume. The second term is the Einstein-Hilbert curvature scalar, governing gravitational dynamics. The third term is the von Neumann entropy density weighted by temperature, representing the tendency of systems to evolve toward maximum entropy.

Extremizing this action yields the field equations of the theory, as we develop in Section 3. Variation with respect to the metric produces modified Einstein equations with an entropic stress-energy correction. Variation with respect to the density matrix produces a thermal equilibrium condition. The Unruh temperature emerges naturally from the entanglement structure via the Bisognano-Wichmann theorem [13].

Remark 2.1 (Microfoundation: Entanglement Equilibrium). The Entropic Action Principle is not an independent postulate but emerges from a more fundamental principle: *entanglement equilibrium in causal diamonds*. Following Jacobson's thermodynamic derivation of Einstein's equations [14], consider a small causal diamond D with boundary area A and bulk entanglement entropy S_{bulk}. The first law of entanglement (Bisognano-Wichmann theorem) gives $\delta S_{\text{bulk}} = \delta\langle K \rangle$, where $K = 2\pi \int_{B_\ell} [(\ell^2 - r^2)/(2\ell)] T_{00}\, dV$ is the modular Hamiltonian. The Raychaudhuri equation applied to the null boundary gives $\delta A \propto -\ell^{d+1} G_{00}$. Demanding stationarity of generalized entropy,

$$\delta S_{\text{gen}} = \frac{\delta A}{4G\hbar} + \delta S_{\text{bulk}} = 0, \tag{5}$$

yields Einstein's equations $G_{\mu\nu} = 8\pi G T_{\mu\nu}$ without postulating an action—the geometric and matter prefactors cancel exactly.

The Entropic Action Principle represents the *effective coarse-grained description* of this microscopic equilibrium when integrated over all causal diamonds. Crucially, the parameter β is the *modular temperature* associated with the local causal diamond—not a global thermal bath. For accelerated observers, $\beta = 2\pi c/a$ gives the Unruh temperature; near black hole horizons, $\beta = 2\pi/\kappa$ gives the Hawking temperature; in flat space far from horizons, $\beta \to \infty$ (zero temperature, pure state). This interpretation resolves the apparent tension between the Gibbs state result $\rho \propto e^{-\beta H}$ and the manifestly non-thermal state of the universe: the "thermality" is local and modular, not global.

2.3 Axiom III: Scale-Dependent Unification

The third axiom addresses the transition between quantum and classical descriptions. At microscopic scales, quantum mechanics provides the accurate description; at macroscopic scales, classical general relativity suffices. The axiom asserts that these descriptions are not in conflict but interpolate smoothly as a function of scale.

Axiom 2.3 (Scale-Dependent Unification)**.** *Physical observables interpolate smoothly between quantum and geometric descriptions via a scale-dependent weighting:*

$$\boxed{\mathcal{O}_{unified}(x) = \rho_{QM}(x) \cdot f\left(\frac{r}{\ell_P}\right) + \rho_{GR}(x) \cdot \left[1 - f\left(\frac{r}{\ell_P}\right)\right]} \tag{6}$$

where $f(x) = 1/(1+x^2)$ *is an interpolating function and* $\ell_P = \sqrt{G\hbar/c^3}$ *is the Planck length.*

Remark 2.2 (Interpolation Function). The function $f(x) = 1/(1+x^2)$ is phenomenologically motivated by renormalization group considerations. Consider a beta function of logistic form $\beta(g) = -g(1-g)$, which has UV fixed point $g = 0$ and IR fixed point $g = 1$. The RG trajectory connecting them has profile $g(\mu) = 1/(1+(\mu/\mu_*)^2)$ where μ_* is the crossover scale. Identifying $\mu_* = 1/\ell_P$ gives the stated form. This derivation is heuristic: alternative interpolation functions satisfying $f(0) = 1$, $f(\infty) = 0$, and smoothness would give qualitatively similar physics. The specific form is adopted for definiteness and should be regarded as a phenomenological choice rather than a rigorous derivation.

This axiom has several important consequences. It implies the existence of a minimum measurable length, since the quantum and geometric descriptions cannot be simultaneously arbitrarily precise. It also leads to modified dispersion relations for particles propagating through Planck-scale structured spacetime, as we derive in Section 4. These modifications, while small, may be detectable through observations of high-energy astrophysical sources.

2.4 Derived: Observer-Dependent Horizons

The relationship between quantum and gravitational uncertainties is not a separate axiom but a consequence of Axiom I together with standard horizon thermodynamics. The Heisenberg uncertainty principle $\Delta E \cdot \Delta t \geq \hbar/2$ governs quantum measurements; the Unruh effect establishes that an accelerating observer perceives a thermal bath at temperature $T = \hbar a/(2\pi c k_B)$. Applying the generalized entropy of Axiom I to a Rindler horizon and using the Unruh relation yields an equivalence between quantum and gravitational uncertainties.

Theorem 2.4 (Observer-Dependent Horizon Principle)**.** *From Axiom I applied to Rindler horizons, together with horizon thermodynamics, quantum and gravitational uncertainties are equivalent manifestations of the same underlying physics:*

$$\boxed{\Delta E \cdot \Delta t \geq \frac{\hbar}{2} \quad \Longleftrightarrow \quad a \cdot \Delta x \geq \frac{c^2}{2}} \tag{7}$$

where a *is proper acceleration.*

An accelerating observer has a Rindler horizon at distance c^2/a; the gravitational uncertainty $a \cdot \Delta x \geq c^2/2$ can be interpreted as a statement about the minimum distance from this horizon, while the quantum uncertainty $\Delta E \cdot \Delta t \geq \hbar/2$ becomes a statement about the energy fluctuations associated with it. The derivation relies on the Unruh result as established external physics; a framework in which that input is modified (for example, doubly special relativity) need not satisfy Eq. (7). In Section 5, we use this principle to obtain the generalized uncertainty principle, combining quantum and gravitational contributions to position-momentum uncertainty.

2.5 Derived: Holographic Information Bound

The holographic principle, proposed by 't Hooft [15] and developed by Susskind [16] and Bousso [17], asserts that the maximum entropy in a region is bounded by the area of its boundary, not its volume. Within the framework it is a theorem following from Axiom I together with the generalized second law of thermodynamics.

Theorem 2.5 (Holographic Bound)**.** *From Axiom I (Generalized Entropy Conservation) and the Generalized Second Law:*

$$\boxed{S_{\max} \leq \frac{A}{4\ell_P^2}} \tag{8}$$

Sketch. Axiom I fixes the geometric entropy to $A/(4\ell_P^2)$ and conserves $S_{\text{gen}} = S_{\text{vN}} + A/(4\ell_P^2)$. The GSL requires S_{gen} to be non-decreasing. Combining these with the requirement that S_{matter} cannot exceed the horizon capacity yields the bound. □

The holographic bound fundamentally constrains the information content of spacetime regions and, when applied to cosmological horizons, yields the holographic dark energy treated in companion work [7].

2.6 Derived: Semiclassical Duality Correspondence

We now state the central physical result of the framework: how matter superpositions couple to geometry in the semiclassical regime. Because Axiom I ties entanglement to geometric area, changes in quantum state must be accompanied by changes in geometry. We make this precise through the Semiclassical Duality Correspondence, a theorem following from Axioms I and II in the semiclassical regime.

Proposition 2.6 (Semiclassical Matter-Geometry Entanglement)**.** *In the semiclassical regime, superpositions of matter states produce entangled matter-geometry states:*

$$\boxed{|\Psi\rangle = \sum_n c_n |\psi_n\rangle \quad \Longrightarrow \quad |\Psi_{total}\rangle = \sum_n c_n |\psi_n\rangle \otimes |\alpha^{(n)}\rangle} \tag{9}$$

where $|\alpha^{(n)}\rangle$ are gravitational coherent states with expectation value $\langle\alpha^{(n)}|\hat{h}_{\mu\nu}|\alpha^{(n)}\rangle = h_{\mu\nu}^{(n)}$ satisfying the linearized Einstein equations sourced by $|\psi_n\rangle$.

This result captures the essence of Quantum-Geometric Correspondence. A matter state in superposition does not source a single classical geometry; instead, each branch of the superposition is correlated with its corresponding geometric perturbation. The total state is entangled: matter and geometry cannot be described independently. The mathematical framework underlying this correspondence, including the definition of gravitational coherent states and the semiclassical validity regime, is developed in Appendix B. When an external observer traces over the geometric degrees of freedom (which are inaccessible to typical laboratory measurements), the matter state appears to undergo decoherence—the gravitational decoherence analyzed in Part II.

2.7 Hypothesis: The Gravitational Information Axiom

Finally, we state a principle governing the *rate* at which information is transferred between matter and geometric degrees of freedom. We emphasize that this is a hypothesis, not one of the three primitive axioms: the axioms fix the energy scale of gravitational decoherence, but not the coefficient relating that scale to the rate. The Diósi-Penrose formula for gravitational decoherence [5, 6] suggests that the gravitational self-energy $E_{\text{grav}} = GM^2/d$ sets the energy scale; the Margolus-Levitin bound establishes that the maximum rate of quantum state evolution is $2E/(\pi\hbar)$. We hypothesize that gravitational information transfer saturates this bound.

Principle 2.7 (Gravitational Information Axiom (GIA))**.** *Gravitational information transfer between matter and geometric degrees of freedom saturates the Margolus-Levitin bound:*

$$\boxed{\frac{dI_{S:G}}{dt} = \frac{2E_{grav}}{\pi\hbar}, \quad E_{grav} = \frac{GM^2}{d}} \tag{10}$$

This gives G^1 scaling for decoherence, rather than the perturbative G^2 scaling.

This hypothesis is supported by multiple considerations: saturation of the Margolus-Levitin bound, the Diósi-Penrose conjecture, consistency with Axiom I (Generalized Entropy Conservation), and a derivation from the constrained Feynman-Vernon influence functional in linearized gravity (Section 9). The derivation shows that imposing the Wheeler-DeWitt constraint on the initial state replaces the G^2 noise-kernel mechanism with a G^1 coherent-state-overlap mechanism. Standard perturbative QFT calculations, which use an unconstrained product initial state, give G^2 scaling. Both results are correct for their respective initial conditions. We develop this in detail in Part II and discuss its status in Section 12.

2.8 Axiomatic Structure Summary

Primitive Axioms (independent, cannot be derived):

Axiom	**Content**	**Physical Basis**
I	Generalized Entropy Conservation	Unitarity + holography
II	Entropic Action Principle	Entanglement equilibrium
III	Scale-Dependent Unification	RG flow

Derived Results (theorems following from the axioms):

Result	**Content**	**Derived From**
Theorem 2.4	Observer-Dependent Horizons	Axiom I + horizon thermodynamics
Theorem 2.5	Holographic Bound $S \leq A/(4\ell_P^2)$	Axiom I + GSL
Prop. 2.6	Semiclassical Duality Correspondence	Axioms I + II

Separate Hypothesis (fixes the decoherence *rate*, not a primitive axiom):

Statement	**Content**	**Status**
GIA	Gravitational Information Axiom	Hypothesis (G^1 scaling)

The three primitive axioms are logically independent: each can be violated while the others hold, as we demonstrate through explicit countermodels in Appendix A.

Remark 2.3 (Relation to the expanded six-statement presentation). Earlier presentations of this framework listed a larger set of statements for pedagogical transparency: Generalized Entropy Conservation (Axiom I) was split into separate "Information Conservation" and "Entanglement-Geometry Correspondence" statements, and the Observer-Dependent Horizon Principle and Holographic Bound were listed alongside the axioms rather than as derived theorems—yielding a "six-axiom plus duality-correspondence" structure. That structure is entirely recovered here: the split statements are the two facets of Axiom I discussed above, and the horizon and holographic results are Theorems 2.4 and 2.5. The minimal three-axiom formulation is canonical; the expanded enumeration is a derived re-packaging of the same physical content.

3 Entropic Dynamics

The Entropic Action Principle (Axiom II) provides a unified variational formulation for coupled matter-geometry systems. In this section, we extremize the action to derive the field equations of the theory. The procedure follows standard variational methods, but the inclusion of the entropic term leads to modifications of both the Einstein equations and the equilibrium condition for matter.

We begin with the entropic action as stated in Eq. (4). The action depends on two independent variables: the spacetime metric $g_{\mu\nu}$ and the matter density matrix ρ. Physical configurations correspond to extrema of this action, obtained by requiring that variations with respect to both variables vanish. We consider these variations in turn.

Varying the action with respect to the metric $g_{\mu\nu}$ yields the gravitational field equations. The variation of the Einstein-Hilbert term produces the Einstein tensor $G_{\mu\nu}$ through the standard calculation. The variation of the matter Hamiltonian term produces the expectation value of the stress-energy tensor. The entropic term contributes an additional piece proportional to the metric times the von Neumann entropy. Collecting these contributions and requiring $\delta S/\delta g_{\mu\nu} = 0$, we obtain the modified Einstein equations:

$$\boxed{G_{\mu\nu} = \frac{8\pi G}{c^4}\left(\langle \hat{T}_{\mu\nu}\rangle + \frac{S_{\text{vN}}}{\beta} g_{\mu\nu}\right)} \tag{11}$$

The first term on the right-hand side is the standard source term from matter: the expectation value of the stress-energy tensor in the quantum state ρ. The second term is an entropic correction: a contribution proportional to the von Neumann entropy $S_{\text{vN}} = -\text{Tr}(\rho \ln \rho)$ weighted by the inverse temperature $\beta^{-1} = k_B T$. This entropic stress-energy has the form of a perfect fluid with equation of state $p = -\rho_{\text{ent}}$, where $\rho_{\text{ent}} \equiv S_{\text{vN}}/\beta$ is the energy density of the entropic term, precisely the equation of state for a cosmological constant.

The physical interpretation of this result is significant. In thermal equilibrium, entropic effects contribute to the effective stress-energy sourcing gravity. At low temperatures (large β), the entropic contribution is suppressed. At high temperatures, it becomes increasingly important. This provides a natural mechanism for entropy-driven gravitational effects in hot, dense environments such as the early universe.

We now turn to the matter equations. Varying the action with respect to the density matrix ρ and requiring $\delta S/\delta \rho = 0$ yields the equilibrium condition for matter:

$$\boxed{\rho = \frac{e^{-\beta \hat{H}[g]}}{Z[g]}} \tag{12}$$

where $Z[g] = \text{Tr}(e^{-\beta \hat{H}[g]})$ is the partition function and $\hat{H}[g]$ is the matter Hamiltonian in the background geometry $g_{\mu\nu}$. This is the Gibbs thermal state at temperature $T = 1/(k_B\beta)$. The matter system equilibrates to a thermal distribution determined by the local temperature and the Hamiltonian.

The coupled equations (11) and (12) must be solved self-consistently. The geometry $g_{\mu\nu}$ enters the matter Hamiltonian $\hat{H}[g]$, which determines the equilibrium state ρ. The state ρ then sources the geometry through the stress-energy tensor. Finding a solution requires iterating until convergence, as we discuss in Appendix C. In the weak-field regime, the self-consistency

map is a contraction, guaranteeing existence and uniqueness of solutions.

A natural question arises: what determines the temperature β^{-1} appearing in the action? In ordinary thermodynamics, temperature is determined by the environment—a heat bath with which the system is in contact. In the present context, however, the system under consideration includes gravity, and there may be no external heat bath. The resolution comes from the Bisognano-Wichmann theorem [13], which establishes that the vacuum state of a quantum field theory, when restricted to a Rindler wedge (the region accessible to a uniformly accelerating observer), is a thermal state at the Unruh temperature.

The Unruh temperature is given by:

$$\boxed{T = \frac{\hbar a}{2\pi c k_B}} \tag{13}$$

where a is the proper acceleration. This result connects acceleration, temperature, and quantum mechanics: an accelerating observer perceives the quantum vacuum as a thermal bath. The temperature is determined not by an external environment but by the observer's acceleration and, more generally, by the entanglement structure of the quantum state across the observer's horizon.

Within the Quantum-Geometric Correspondence framework, the Unruh temperature is not merely an observed effect but a fundamental ingredient. The inverse temperature β in the entropic action is determined by the local acceleration through Eq. (13). In a general curved spacetime, the local temperature varies according to the Tolman relation, which ensures thermal equilibrium in the presence of gravitational redshift. The temperature appearing in Eq. (4) is thus not a free parameter but is fixed by the entanglement structure of the quantum fields and the geometry of spacetime.

In this construction, the inverse temperature β in the entropic action is fixed by the local acceleration (Unruh) and gravitational redshift (Tolman) rather than by a free parameter, and black hole thermodynamics, with its temperature determined by surface gravity, is the special case in which the relevant horizon is an event horizon.

4 Scale-Dependent Unification

The Scale-Dependent Unification axiom (Axiom III) asserts that quantum and geometric descriptions interpolate smoothly as a function of the length scale. This interpolation has concrete physical consequences: the existence of a minimum measurable length, and modified dispersion relations for particles propagating through Planck-scale structured spacetime. In this section, we present these consequences, which follow from the axiom given standard physical arguments, and discuss their experimental signatures.

These results follow from the fact that position and momentum measurements cannot simultaneously achieve arbitrary precision when gravitational effects are included. The standard Heisenberg uncertainty principle, $\Delta x \cdot \Delta p \geq \hbar/2$, constrains measurements of position and momentum but places no lower bound on position uncertainty alone—in principle, arbitrarily precise position measurements are possible if one accepts correspondingly large momentum uncertainty. Gravity changes this picture. Attempting to localize a particle to very small scales requires concentrating energy in a small region; at some point, the energy density becomes

sufficient to form a black hole, and the position measurement becomes meaningless. This heuristic argument suggests that there exists a minimum length scale below which spatial localization is impossible.

To make this precise, we combine the quantum uncertainty principle with gravitational considerations. The generalized uncertainty principle (GUP) that emerges from this combination has the form:

$$\boxed{\Delta x \geq \frac{\hbar}{2\Delta p} + \frac{\beta_{\mathrm{GUP}} G \Delta p}{2c^3}} \tag{14}$$

where β_{GUP} is a dimensionless parameter of order unity. The first term is the standard quantum contribution, dominant at low momenta. The second term is the gravitational contribution, dominant at high momenta. Together, they imply that position uncertainty cannot be made arbitrarily small.

To find the minimum uncertainty, we minimize Δx with respect to Δp. Setting $d(\Delta x)/d(\Delta p) = 0$ yields $\Delta p_{\mathrm{opt}} = \sqrt{\hbar c^3/(\beta_{\mathrm{GUP}} G)} = \hbar/(\sqrt{\beta_{\mathrm{GUP}}}\,\ell_P)$, where $\ell_P = \sqrt{G\hbar/c^3}$ is the Planck length. Substituting back, we obtain the minimum position uncertainty:

$$\boxed{\Delta x_{\mathrm{min}} = \sqrt{\beta_{\mathrm{GUP}}}\,\ell_P \approx (1.4 \pm 0.5)\,\ell_P \approx (2.3 \pm 0.8) \times 10^{-35}\ \mathrm{m}} \tag{15}$$

where we have used $\beta_{\mathrm{GUP}} = 2$ with an estimated range of 1–4. The minimum length is of order the Planck length, as expected on dimensional grounds, but the precise coefficient depends on the details of the gravitational contribution to uncertainty.

This result implies that spacetime has an effective minimum resolution at the Planck scale. No measurement procedure, however ingenious, can localize an object to better than Planck precision. This is not merely an experimental limitation but a fundamental property of nature reflecting the interplay between quantum mechanics and gravity. The minimum length is sometimes interpreted as evidence for discrete spacetime structure, though the present framework is agnostic on this point—the minimum length emerges from the uncertainty principle rather than from explicit discreteness.

We now turn to the consequences for particle propagation. The GUP implies a modification of the standard commutation relation between position and momentum. In ordinary quantum mechanics, $[\hat{x}, \hat{p}] = i\hbar$. The GUP is consistent with the modified commutator:

$$\boxed{[\hat{x}, \hat{p}] = i\hbar \left(1 + \beta_{\mathrm{GUP}} \frac{\ell_P^2 \hat{p}^2}{\hbar^2}\right)} \tag{16}$$

The correction term becomes significant only when the momentum approaches the Planck scale, $p \sim \hbar/\ell_P$.

This modified commutation relation has consequences for the dispersion relation of particles. The standard relativistic dispersion relation $E^2 = p^2c^2 + m^2c^4$ follows from Lorentz invariance. Planck-scale modifications of the commutation relation lead to corresponding modifications of the dispersion relation. Working to leading order in the correction, we obtain:

$$\boxed{E^2 = p^2c^2 \left(1 + \xi \frac{p^2 \ell_P^2}{\hbar^2}\right) + m^2c^4} \tag{17}$$

where $\xi = \beta_{\text{GUP}} \sim O(1)$ is the dispersion coefficient. The correction is suppressed by $(p\ell_P/\hbar)^2$, making it negligible for ordinary particles but potentially detectable for ultra-high-energy photons.

For massless particles such as photons, the modified dispersion relation implies an energy-dependent group velocity. Taking the derivative $v = dE/dp$ and working to leading order, we find:

$$\boxed{v = c\left(1 - |\xi|\frac{E^2}{E_P^2}\right)} \tag{18}$$

where $E_P = \sqrt{\hbar c^5/G} \approx 1.22 \times 10^{19}$ GeV is the Planck energy and we have adopted the subluminal convention ($\xi > 0$, corresponding to $v < c$) consistent with observational constraints. Higher-energy photons travel slightly slower than lower-energy photons. The effect is minuscule—even for GeV photons, the velocity differs from c by only one part in 10^{28}—but it accumulates over cosmological distances.

This velocity difference leads to a measurable time delay between photons of different energies emitted simultaneously from the same source. Consider two photons with energies E_1 and E_2 emitted from a source at distance L. The higher-energy photon travels more slowly, arriving later than the lower-energy photon. The time delay is:

$$\boxed{\Delta t = \xi\frac{E_1^2 - E_2^2}{E_P^2} \cdot \frac{L}{c}} \tag{19}$$

For a gamma-ray burst at cosmological distance ($L \sim 10^{26}$ m) with GeV photons ($E \sim 10^9$ eV), this predicts a time delay of order $\Delta t \sim 0.2$ s, potentially observable with current instruments.

The E^2 scaling of the dispersion correction is a distinctive signature of the framework. Alternative approaches to quantum gravity modifications predict different scalings: some loop quantum gravity scenarios predict E^1 corrections, while other effective theories predict E^3 or higher. The observed scaling, if measured, would therefore discriminate between different theoretical approaches. Current observations from gamma-ray bursts have not detected significant time delays, placing bounds $|\xi| \lesssim 1$ for E^2 corrections [18]. These bounds are consistent with the framework's predictions and motivate continued observations of high-energy astrophysical sources.

5 Observer-Dependent Horizons

The Observer-Dependent Horizon Principle (Theorem 2.4), derived from Axiom I together with horizon thermodynamics, establishes an equivalence between quantum uncertainties and gravitational horizons. This equivalence has two major consequences that we develop in this section: the generalized uncertainty principle, which follows from the axioms combined with the modified commutation relation, and vacuum birefringence arising from non-commutative spacetime structure at the Planck scale.

The starting point is the equivalence stated in Eq. (7): the quantum uncertainty relation $\Delta E \cdot \Delta t \geq \hbar/2$ is physically equivalent to the gravitational relation $a \cdot \Delta x \geq c^2/2$, where a is proper acceleration. To understand this equivalence, consider an observer undergoing uniform acceleration a. According to the Unruh effect, such an observer perceives the quantum vacuum

as a thermal bath at temperature $T = \hbar a/(2\pi c k_B)$. The observer also has a Rindler horizon at proper distance $d_H = c^2/a$ behind them—a surface from beyond which no signal can reach the observer. The gravitational uncertainty $a \cdot \Delta x \geq c^2/2$ can be interpreted as stating that the observer cannot probe distances closer than half the horizon distance.

The connection to quantum uncertainty proceeds through dimensional analysis. Using the Unruh temperature to relate acceleration to energy ($k_B T = \hbar a/(2\pi c)$, so $a = 2\pi c k_B T/\hbar$) and the relation $\Delta E \sim k_B T$, the gravitational relation $a \cdot \Delta x \geq c^2/2$ becomes $\Delta E \cdot \Delta x \geq \hbar c/(4\pi)$. With the substitution $\Delta t \sim \Delta x/c$, this recovers the form of the quantum uncertainty principle. The numerical factor differs by π from the standard quantum relation; the factor of π reflects the heuristic nature of this dimensional matching and is not part of the claimed result.

The Observer-Dependent Horizon Principle, combined with the modified commutation relation Eq. (16), provides an independent route to the generalized uncertainty principle. The derivation follows from the Robertson uncertainty relation, which states that for any two observables $\hat{A}$ and $\hat{B}$, the product of their uncertainties satisfies $\Delta A \cdot \Delta B \geq |\langle[\hat{A}, \hat{B}]\rangle|/2$. Applying this to position and momentum with the modified commutator yields:

$$\Delta x \cdot \Delta p \geq \frac{\hbar}{2}\left(1 + \beta_{\mathrm{GUP}} \frac{\ell_P^2 \langle \hat{p}^2 \rangle}{\hbar^2}\right) \tag{20}$$

For a minimum-uncertainty state, $\langle \hat{p}^2 \rangle \approx (\Delta p)^2$, giving the GUP in the form already stated as Eq. (14). This derivation shows that the GUP is not merely a heuristic but follows from the modified algebraic structure implied by scale-dependent unification and observer-dependent horizons.

We now turn to a more dramatic consequence of Planck-scale physics: vacuum birefringence. The modified commutation relation between position and momentum suggests a more general non-commutativity of spacetime coordinates themselves. In theories where spacetime structure is affected by quantum gravity, position operators may fail to commute:

$$\boxed{[\hat{x}^\mu, \hat{x}^\nu] = i\theta^{\mu\nu}, \quad \theta^{\mu\nu} \sim \ell_P^2\, \Theta^{\mu\nu}} \tag{21}$$

where $\Theta^{\mu\nu}$ is a dimensionless antisymmetric tensor characterizing the non-commutativity. The magnitude of the non-commutativity is set by the Planck area ℓ_P^2, as expected on dimensional grounds.

Non-commutative spacetime breaks Lorentz invariance in a specific way. The tensor $\Theta^{\mu\nu}$ defines preferred directions in spacetime, leading to anisotropic propagation of light. In particular, left-handed and right-handed circularly polarized photons couple differently to the non-commutative structure and therefore propagate at different speeds. This phenomenon is vacuum birefringence: the vacuum itself acts as a birefringent medium for light.

The physical picture is the following. In ordinary electromagnetism, Maxwell's equations treat left and right circular polarizations identically. Non-commutative spacetime introduces corrections to Maxwell's equations that depend on the photon helicity. The corrections are suppressed by powers of E/E_P, where E is the photon energy and E_P is the Planck energy, but they accumulate over large distances. A photon travelling through non-commutative spacetime therefore experiences a rotation of its polarization plane, with the rotation angle depending on energy and distance.

The scaling of this effect with energy is determined by the structure of the non-commutative

corrections. In the framework presented here, dimensional analysis and symmetry considerations lead to a rotation angle scaling as E^3:

$$\boxed{\Delta\phi \approx \Delta\eta \left(\frac{E}{E_P}\right)^3 \cdot \frac{L}{\ell_P}} \tag{22}$$

where $\Delta\phi$ is the polarization rotation angle, L is the propagation distance, E is the photon energy, and $|\Delta\eta| \sim O(1)$ is a dimensionless coefficient depending on the details of the non-commutative structure. The E^3 scaling arises because the leading E^1 and E^2 corrections are forbidden by symmetry considerations in the present framework.

To estimate the observable effect, consider gamma-ray bursts (GRBs) at cosmological distances. A GRB at redshift $z \sim 2$–3 corresponds to a comoving distance of order $L \sim 10^{26}$ m, or approximately 10^{61} Planck lengths. For photons with energy $E \sim 10$ MeV, the ratio $E/E_P \sim 10^{-22}$. Combining these factors:

$$\boxed{\Delta\phi \sim 5 \times 10^{-3} \text{ rad} \sim 0.3^\circ} \tag{23}$$

This is a small but potentially measurable effect. GRB polarimetry has achieved sensitivity at the few-degree level, and next-generation instruments may reach the precision needed to detect or constrain effects at the 0.3° level.

The E^3 scaling is a distinctive signature of the framework. Alternative approaches to Lorentz-violating physics predict different scalings: the Myers-Pospelov effective theory predicts E^2 birefringence, while the Standard Model Extension (SME) includes operators leading to E^1 and E^2 effects. Observational detection of the scaling would therefore discriminate between theoretical approaches. Current GRB polarization observations have not detected significant birefringence, but the limits are not yet stringent enough to constrain E^3 effects at the level predicted here [19]. Continued observations with instruments such as IXPE [20] and future dedicated polarimeters will improve these constraints.

The absence of detected birefringence to date is consistent with the framework's predictions, which place the effect at the edge of current observational capabilities. A positive detection would be a dramatic confirmation of Planck-scale physics; continued non-detection would place increasingly stringent bounds on the coefficient $\Delta\eta$ and potentially falsify certain ranges of parameters. Either outcome would provide valuable information about the structure of spacetime at the smallest scales.

Part II
Gravitational Decoherence

6 The Diósi-Penrose Mechanism

Part I established that, in the semiclassical regime, a matter superposition becomes entangled with a superposition of gravitational field configurations (the Semiclassical Duality Correspondence, Proposition 2.6). Tracing over the inaccessible geometry then decoheres the matter. We now turn to the quantitative content of this effect, which is precisely the Diósi-Penrose hypothesis:

the classical gravitational self-energy of a spatial superposition directly determines the rate at which that superposition decoheres. This section states the hypothesis precisely, derives its consequences for decoherence timescales, and examines its key features. The microscopic justification of the G^1 rate follows in Sections 9 and 10.

6.1 Gravitational Self-Energy

The Diósi-Penrose gravitational self-energy measures the "difference" between the two geometric configurations:

$$E_G = \frac{G}{2} \int \int \frac{[\rho_1(\mathbf{x}) - \rho_2(\mathbf{x})][\rho_1(\mathbf{y}) - \rho_2(\mathbf{y})]}{|\mathbf{x} - \mathbf{y}|} d^3x \, d^3y \tag{24}$$

where ρ_1 and ρ_2 are the mass densities in the two branches of the superposition. For well-separated point masses ($d \gg R$, where R is the particle radius), this reduces to:

$$E_G \approx \frac{GM^2}{d} \tag{25}$$

We work in this point-mass limit throughout, which is valid for the mesoscopic particles of experimental interest.

6.2 The Diósi-Penrose Hypothesis

The hypothesis can be formulated as follows. Consider a mass distribution that exists in a quantum superposition of two configurations, with mass densities $\rho_1(\mathbf{x})$ and $\rho_2(\mathbf{x})$ in the two branches. The gravitational self-energy defined in Eq. (24) measures the gravitational interaction energy between the "excess" mass in one branch and the "deficit" in the other. For two point masses of mass M separated by distance d, the expression simplifies to the familiar form $E_G = GM^2/d$.

The Diósi-Penrose hypothesis postulates that this gravitational self-energy sets the decoherence rate according to

$$\Gamma_{\text{dec}} = \frac{E_G}{\hbar}. \tag{26}$$

That is, the rate at which coherence is lost between the two branches equals the gravitational energy scale divided by Planck's constant. This is a remarkably direct prescription: no coupling constants beyond G appear, no perturbative expansion is invoked, and no details of the mediating degrees of freedom enter. The hypothesis treats the gravitational self-energy as the fundamental quantity and simply converts it to a rate using the standard quantum-mechanical relation between energy and frequency.

To understand the physical content of this hypothesis, consider a mass M in spatial superposition over distance d, with the initial state

$$|\Psi(t=0)\rangle = \frac{1}{\sqrt{2}} \left(|\mathbf{r}_1\rangle + |\mathbf{r}_2\rangle \right), \quad |\mathbf{r}_1 - \mathbf{r}_2| = d. \tag{27}$$

We work in the regime where the Newtonian approximation is valid ($GM/(c^2 d) \ll 1$), the superposition separation exceeds the particle size ($d \gg r$), and environmental decoherence from photons, gas molecules, and thermal radiation has been suppressed through high vacuum and cryogenic temperatures.

Under these conditions, the Diósi-Penrose mechanism predicts that the off-diagonal elements of the density matrix decay exponentially:

$$\rho_{12}(t) = \rho_{12}(0)e^{-\Gamma t} = \rho_{12}(0)e^{-t/\tau_{\rm dec}}, \tag{28}$$

where the decoherence time is the inverse of the rate given by Eq. (26). For a point mass, this yields

$$\boxed{\tau_{\rm dec} = \frac{\hbar d}{C\,GM^2}}, \qquad \Gamma_{\rm dec} = C\,\frac{GM^2}{\hbar d}, \tag{29}$$

where the coefficient C is of order unity. The precise value of C depends on details that the Diósi-Penrose hypothesis alone does not specify: the geometry of the mass distribution, the regularization scheme used to handle the self-energy of point particles, and the exact relationship between the gravitational energy scale and the decoherence rate. As we show in Section 10, the Margolus-Levitin quantum speed limit bounds C to the window $[2/\pi, 1]$, with natural value $C = 1$ (Markovian dephasing). We take $C = 1$ for numerical estimates, while emphasizing that experiments should primarily test the scaling relations ($\tau \propto M^{-2}$, $\tau \propto d$, $\Gamma \propto G^1$) rather than the absolute coefficient. All explicit rate formulas in this paper set $C = 1$; the residual uncertainty in C should be borne in mind when comparing predicted and observed absolute timescales.

The formula (29) has several notable features that distinguish gravitational decoherence from other mechanisms. First, it requires both $\hbar$ and G—it is genuinely quantum-gravitational in character. Neither classical gravity alone nor quantum mechanics without gravity produces this timescale. The combination $\hbar d/(GM^2)$ is the unique timescale that can be constructed from the available quantities with the correct dimensions.

Second, the predicted decoherence is temperature-independent. Unlike thermal decoherence, which diminishes as $T \to 0$, gravitational decoherence persists at absolute zero. The gravitational self-energy depends only on the mass distribution, not on the thermal state of the system or its environment. This provides a sharp experimental signature: if decoherence rates approach a constant value as temperature is reduced rather than continuing to decrease, gravitational decoherence may be the cause.

Third, the effect is vacuum-independent. Decoherence from scattered photons or gas molecules can be suppressed by improving the vacuum, but gravitational decoherence cannot. It operates in the most perfect vacuum achievable, requiring no photons, no air molecules, no thermal radiation—only the gravitational field itself. Again, this provides an experimental signature: decoherence that persists as vacuum quality improves, at rates consistent with the gravitational prediction, would support the Diósi-Penrose mechanism.

To develop quantitative intuition, we compute the predicted decoherence time for a concrete example: a particle of mass $M = 1\ \mu\text{g} = 10^{-9}$ kg in superposition over $d = 1$ mm $= 10^{-3}$ m. Substituting into Eq. (29) with $C = 1$:

$$\begin{aligned}
\tau_{\rm dec} &= \frac{\hbar d}{GM^2} \\
&= \frac{(1.05 \times 10^{-34}\ \text{J}\cdot\text{s})(10^{-3}\ \text{m})}{(6.67 \times 10^{-11}\ \text{m}^3\text{kg}^{-1}\text{s}^{-2})(10^{-9}\ \text{kg})^2} \\
&\approx 1.6 \times 10^{-9}\ \text{s}.
\end{aligned} \tag{30}$$

A microgram particle delocalized over a millimeter would decohere in about a nanosecond—fast enough to explain why such superpositions are never observed, but not so fast as to be completely inaccessible to future experiments.

The scaling with mass deserves particular attention. The decoherence time decreases as M^{-2}, meaning that doubling the mass reduces the coherence time by a factor of four. This strong mass dependence ensures that macroscopic objects decohere almost instantaneously. A 1 mg particle (one thousand times more massive than our example) would have a decoherence time of 1.6×10^{-15} s, and a 1 g particle would decohere in 1.6×10^{-21} s. By the time we reach human scales—say, 70 kg at 1 m separation—the decoherence time is of order 10^{-28} s, many orders of magnitude shorter than any physical process could create such a superposition.

We close this section by stating the conditions under which the Diósi-Penrose hypothesis would be falsified. The hypothesis makes specific, quantitative predictions that can be tested experimentally:

1. If coherence persists for times exceeding the predicted τ_{dec} by more than a factor of 10^3, accounting for the uncertainty in the coefficient C, the hypothesis in its current form would be ruled out.

2. If decoherence rates are observed to scale as G^2 rather than G^1—that is, if rates are approximately 3×10^{34} times slower than predicted (for the $1\,\mu$g, 1 mm benchmark)—the hypothesis would be falsified in favor of standard quantum field theory predictions.

3. If decoherence rates depend strongly on temperature or vacuum quality, scaling down as these are improved rather than approaching a constant floor, then the observed decoherence is environmental rather than gravitational.

4. If decoherence rates scale as M^{-1} rather than M^{-2}, this would favor Károlyházy's model over Diósi-Penrose, providing discrimination between different proposed gravitational decoherence mechanisms.

These falsification criteria make the Diósi-Penrose hypothesis genuinely scientific: it makes predictions that could be wrong, and it specifies what observations would demonstrate that wrongness.

7 Standard Quantum Field Theory versus Diósi-Penrose

The Diósi-Penrose mechanism and standard quantum field theory make dramatically different predictions for gravitational decoherence rates. This section examines the origin of this discrepancy, which ultimately traces to different assumptions about how gravitational energy scales translate into quantum mechanical rates. The predictions differ by the factor $(M_P/M)^2(d/\ell_P)$, which equals $\sim 3 \times 10^{34}$ for the $1\,\mu$g, 1 mm benchmark, making experimental discrimination possible even with substantial uncertainties.

The comparison is summarized in Table 1. Standard QFT predicts decoherence rates that scale as G^2, while Diósi-Penrose predicts G^1 scaling. For a 1 μg particle in superposition over 1 mm, this difference translates to decoherence times of approximately 10^{-9} s (Diósi-Penrose) versus $\sim 10^{18}$ years (standard QFT)—a factor of $\sim 3 \times 10^{34}$ difference for this benchmark.

We now examine the physical and mathematical origins of each prediction.

In perturbative quantum field theory, decoherence arises from the interaction of a quantum system with its environment. The standard master equation for the reduced density matrix of the system takes the Lindblad form, which for weak coupling to a thermal environment involves a double commutator structure:

$$\frac{d\hat{\rho}_M}{dt} = -\frac{1}{\hbar^2}\int_0^t dt' \,\mathrm{Tr}_{\mathrm{env}}\left\{[\hat{H}_{\mathrm{int}}(t), [\hat{H}_{\mathrm{int}}(t'), \hat{\rho}_M \otimes \hat{\rho}_{\mathrm{env}}]]\right\}. \tag{31}$$

The interaction Hamiltonian appears twice in this expression—once for each commutator—and this mathematical structure determines the scaling of decoherence rates.

For gravitational interactions, the coupling between matter and the gravitational field takes the form

$$\hat{H}_{\mathrm{int}} = \kappa \int d^3x \, T^{\mu\nu}(\mathbf{x})\hat{h}_{\mu\nu}(\mathbf{x}), \tag{32}$$

where $T^{\mu\nu}$ is the stress-energy tensor of the matter, $\hat{h}_{\mu\nu}$ is the quantized metric perturbation, and the coupling constant $\kappa = \sqrt{32\pi G/c^4}$ is proportional to $\sqrt{G}$. Because this interaction Hamiltonian appears twice in the master equation (31), the decoherence rate necessarily scales as

$$\Gamma_{\mathrm{QFT}} \propto \kappa^2 \propto G. \tag{33}$$

But this is only one power of G, so where does the G^2 come from?

The full calculation, carried out by Anastopoulos and Hu [21] and by Blencowe [22], reveals that the decoherence rate scales as G^2 overall. For a 1 μg particle in superposition over 1 mm, this gives decoherence times of order $\sim 10^{18}$ years—effectively infinite for any practical purpose, and certainly far beyond experimental accessibility.

The Diósi-Penrose rate can be derived by imposing the Wheeler-DeWitt constraint on the Feynman-Vernon influence functional, as we show in Section 9. The constraint $\hat{H}_{\mathrm{total}}|\Psi_{\mathrm{phys}}\rangle = 0$ forces each mass configuration to be accompanied by its coherent gravitational field, replacing the product state with an entangled state. The decoherence rate is then determined by the overlap of the coherent gravitational field states:

$$E_G = \frac{GM^2}{d} \tag{34}$$

contains exactly one power of G, and the constrained influence functional yields $\Gamma = E_G/\hbar$ with this G^1 scaling. No double commutator structure appears because the mechanism operates through the coherent-state overlap rather than perturbative Lindblad dynamics.

Physically, one may understand the difference as follows. Standard QFT treats decoherence as arising from virtual graviton exchange between the system and its environment, computed order by order in perturbation theory. Each graviton vertex contributes one power of $\sqrt{G}$, and the leading contribution to decoherence involves two vertices (one emission and one absorption), giving G^1. But the full QFT calculation reveals that this leading term vanishes due to symmetry considerations, and the first non-vanishing contribution comes from higher-order diagrams, yielding G^2.

The Diósi-Penrose approach, by contrast, treats the gravitational self-energy as a classical quantity that sets a quantum timescale. This is analogous to how the time-energy uncertainty relation $\Delta E \cdot \Delta t \gtrsim \hbar$ connects a classical energy scale to a quantum time—but the Diósi-Penrose hypothesis goes further by asserting that this connection is exact (up to order-unity factors)

rather than merely providing a lower bound.

Diósi's original formulation [5] made this structure explicit by postulating a classical stochastic noise field with correlator

$$\langle \Phi(\mathbf{x}, t)\Phi(\mathbf{x}', t')\rangle = \frac{G\hbar}{|\mathbf{x} - \mathbf{x}'|}\delta(t - t'). \tag{35}$$

This correlator contains exactly one power of G, and it is designed to produce G^1 decoherence rates by construction. The noise field couples to the mass density, and its stochastic fluctuations drive the loss of coherence between different mass configurations.

Which prediction does nature realize? Both G^1 and G^2 are derived results—they differ in the initial state, not in the approximation scheme. The G^2 result uses an unconstrained product state; the G^1 result uses a Wheeler-DeWitt-constrained entangled state (Section 9). The physical question is whether gravity imposes its constraint on the initial state. The enormous difference between the two predictions makes this an experimentally decidable question. If experiments in the nanogram-to-microgram mass range observe decoherence on timescales of milliseconds to nanoseconds, this would confirm G^1 scaling and the relevance of the Wheeler-DeWitt constraint. If coherence persists for times consistent with G^2 predictions, the product-state treatment would be validated.

The two scenarios have very different implications for fundamental physics. If G^1 scaling is confirmed, it would suggest that gravity has a special character at the quantum-classical interface—that the classical gravitational self-energy directly enters quantum dynamics in a way that is not captured by perturbative graviton exchange. This might indicate that gravity is fundamentally classical, or that there are non-perturbative quantum gravitational effects that enhance decoherence rates far above the perturbative prediction.

If G^2 scaling is confirmed, gravity would be "just another quantum field" at the level of decoherence physics. The gravitational interaction would produce decoherence through the same Lindblad mechanism as any other environmental coupling, with no special status. The predicted decoherence times would be so long as to be experimentally irrelevant, and the classicality of macroscopic objects would have to be explained entirely through conventional environmental decoherence.

Either outcome would be scientifically valuable. The question of whether gravity requires special treatment in quantum mechanics, or whether it can be quantized in the same manner as other fields, is one of the central open problems in theoretical physics. Experimental measurement of gravitational decoherence rates would provide direct evidence bearing on this question.

Table 1 summarizes the key differences between the two approaches.

	Standard QFT	**Diósi-Penrose**
Mechanism	Graviton exchange	Coherent-state overlap
G-scaling	$\Gamma \propto G^2$	$\Gamma \propto G^1$
d-scaling	$\Gamma \propto d^{-2}$	$\Gamma \propto d^{-1}$
Initial state	Unconstrained product	WDW-constrained entangled
Derivation	Perturbative QFT	Constrained FV (Sec. 9)

Table 1. *Detailed comparison of the two approaches to gravitational decoherence.*

We note that the d-scaling also differs: d^{-2} for QFT versus d^{-1} for Diósi-Penrose. In principle this provides another experimental discriminant, though the mass scaling is likely easier to test

in practice.

8 The Standard Feynman-Vernon Influence Functional

Section 7 contrasted the G^1 and G^2 predictions at the conceptual level. We now make the comparison precise, beginning with the standard (unconstrained) derivation of gravitational decoherence via the Feynman-Vernon influence functional [23, 24]. This sets the stage for the constrained calculation below (Section 9), where imposing the Wheeler-DeWitt constraint changes the scaling from G^2 to G^1.

8.1 Setup

Consider a point mass M with center-of-mass coordinate q, coupled to the quantized linearized gravitational field $h_{\mu\nu}$. The total action separates into three pieces:

$$S[q,h] = S_M[q] + S_G[h] + S_{\rm int}[q,h], \tag{36}$$

where S_M is the free matter action, S_G is the free graviton action (the linearized Einstein-Hilbert action for $h_{\mu\nu}$), and the interaction takes the form

$$S_{\rm int}[q,h] = \frac{\kappa}{2}\int d^4x\, T^{\mu\nu}(x;q)\, h_{\mu\nu}(x), \tag{37}$$

with coupling constant

$$\kappa = \sqrt{\frac{32\pi G}{c^4}}\,. \tag{38}$$

The stress-energy tensor $T^{\mu\nu}$ depends on the matter trajectory $q(t)$, and the coupling $\kappa \propto \sqrt{G}$ sets the perturbative expansion parameter.

8.2 The reduced density matrix

We wish to compute the reduced density matrix of the mass after tracing over the gravitational field. In the path-integral formulation, this takes the Feynman-Vernon form [23]:

$$\rho_M(q_f,q_f';t) = \int \mathcal{D}q^+\,\mathcal{D}q^-\;\exp\!\Big(\frac{i}{\hbar}\big[S_M[q^+]-S_M[q^-]\big]\Big)\,\mathcal{F}[q^+,q^-]\;\rho_M(q_i,q_i';0), \tag{39}$$

where q^+ and q^- are the forward and backward paths of the mass, and the influence functional $\mathcal{F}$ encodes the entire effect of the gravitational environment:

$$\mathcal{F}[q^+,q^-] = \int \mathcal{D}h^+\,\mathcal{D}h^-\;\exp\!\Big(\frac{i}{\hbar}\big[S_G[h^+]+S_{\rm int}[q^+,h^+]-S_G[h^-]-S_{\rm int}[q^-,h^-]\big]\Big)\;\rho_E(h_i,h_i'). \tag{40}$$

Here ρ_E is the initial state of the gravitational field.

8.3 The product-state assumption

The standard treatment [23, 24, 21, 22] assumes the total initial state is a product:

$$|\Psi(0)\rangle = |\psi_{\rm matter}\rangle \otimes |0_{\rm grav}\rangle\,, \tag{41}$$

where $|0_{\rm grav}\rangle$ is the graviton vacuum. This is the standard assumption in open quantum systems: the system and environment begin unentangled, and the environment starts in its ground state.

With this choice, the influence functional can be evaluated exactly because the graviton path integral is Gaussian. Defining the difference variable $\Delta q(t) = q^+(t) - q^-(t)$, the imaginary part of the influence phase—responsible for decoherence—takes the noise-kernel form [24, 21]:

$$\mathrm{Im}\,\Phi[q^+, q^-] = \frac{1}{2\hbar}\int_0^t ds \int_0^t ds'\; \Delta T^{\mu\nu}(s)\; N_{\mu\nu\alpha\beta}(s-s')\; \Delta T^{\alpha\beta}(s'), \tag{42}$$

where $\Delta T^{\mu\nu}(s) = T^{\mu\nu}(q^+(s)) - T^{\mu\nu}(q^-(s))$ is the stress-energy difference between the two paths, and $N_{\mu\nu\alpha\beta}$ is the graviton noise kernel—the symmetrized (Hadamard) two-point function of the gravitational field:

$$N_{\mu\nu\alpha\beta}(x, x') = \frac{\kappa^2}{4}\,\langle\{h_{\mu\nu}(x),\, h_{\alpha\beta}(x')\}\rangle_0\,. \tag{43}$$

8.4 G-counting: why the standard result scales as G^2

The G-scaling of the decoherence rate is most transparent in the equivalent master-equation formulation [21]:

$$\frac{d\hat{\rho}_M}{dt} = -\frac{1}{\hbar^2}\int_0^t dt'\; \mathrm{Tr}_{\rm grav}[H_{\rm int}(t),\, [H_{\rm int}(t'),\, \hat{\rho}_M \otimes |0\rangle\langle 0|]], \tag{44}$$

where $H_{\rm int} = (\kappa/2)\int d^3x\, T^{\mu\nu}h_{\mu\nu}$. The G-counting proceeds as follows. The double commutator contains two insertions of $H_{\rm int}$, each carrying one factor of $\kappa \propto \sqrt{G}$, giving $\kappa^2 \propto G$. Tracing over the graviton vacuum produces the Hadamard two-point function $\langle 0|\{h_{\mu\nu}(x), h_{\alpha\beta}(x')\}|0\rangle$; for the canonically normalized graviton field, this propagator carries no explicit factor of G. The G-scaling from the coupling and trace is therefore G^1.

However, the full calculation involves contracting the noise kernel with the stress-energy tensor difference $\Delta T^{\mu\nu} \propto M$ and integrating over the graviton spectral density. For a non-relativistic mass, the relevant frequency integrals contribute matter-dependent factors that bring the total to G^2. Physically, each graviton vertex contributes $\sqrt{G}$, and the leading (two-vertex) decoherence process involves one emission and one absorption, giving G^1 from the vertices; the graviton propagator connecting them, when contracted with the stress-energy sources, contributes the additional G through the Newtonian potential $\Phi_N \propto GM/r$. The net result is [21, 22]

$$\Gamma_{\rm QFT} \propto G^2. \tag{45}$$

The full result, computed by Anastopoulos and Hu [21] and by Blencowe [22], takes the form

$$\boxed{\Gamma_{\rm QFT} \sim \frac{G^2M^4}{\hbar^3 d^2}} \tag{46}$$

(suppressing order-unity numerical prefactors and factors of c). For a 1 μg mass separated by 1 mm, this gives $\tau_{\rm QFT} = 1/\Gamma_{\rm QFT} \sim 10^{18}$ years—effectively infinite, and far beyond any foreseeable experimental reach.

8.5 Identification of the critical assumption

The G^2 scaling can be traced directly to the product-state assumption (41). In the noise-kernel mechanism, decoherence arises because the two branches of the superposition emit slightly different graviton fields, and the growing distinguishability of these emitted fields degrades coherence. This is a *dynamical* process: entanglement between the mass and the gravitational field must be *generated* through the interaction, starting from zero. The rate of entanglement generation is set by $H_{\rm int}^2 \propto G$, and the propagation of the emitted gravitons through the vacuum contributes another factor of G, yielding G^2 overall.

However, the product state (41) violates the linearized Wheeler-DeWitt constraint. A mass at position q must carry its Newtonian gravitational field—the graviton vacuum $|0_{\rm grav}\rangle$ is not a physical state for a system containing matter. The constraint demands that the initial state be *entangled*: each branch of the superposition must be dressed by its own coherent gravitational field configuration.

In Section 9, we impose this constraint and show that it replaces the noise-kernel mechanism (dynamical entanglement generation $\to G^2$) with a coherent-state-overlap mechanism (pre-existing entanglement manifestation $\to G^1$). The physical decoherence rate is set not by how fast gravitons are emitted, but by how fast the pre-existing gravitational dressing of the two branches becomes distinguishable.

9 The Constrained Influence Functional

We now develop the central result of this paper: the influence functional for gravitational decoherence when the Wheeler-DeWitt constraint is properly imposed on the Schwinger-Keldysh path integral. The constraint changes *both* the initial state and the structure of the functional integral itself, replacing the noise-kernel mechanism of Section 8 (which gives G^2) with a coherent-state overlap mechanism (which gives G^1).

9.1 The Wheeler-DeWitt constraint in linearized gravity

In canonical quantum gravity, physical states must satisfy the Hamiltonian constraint [25]:

$$\hat{H}_{\rm total}\,|\Psi_{\rm phys}\rangle = 0\,. \tag{47}$$

In the linearized (Newtonian) limit, the total Hamiltonian decomposes as $\hat{H}_{\rm total} = \hat{H}_{\rm matter} + \hat{H}_{\rm grav} + \hat{H}_{\rm int}$, and the constraint reduces to the operator Poisson equation:

$$\nabla^2\hat{\Phi}(\mathbf{x}) = 4\pi G\,\hat{\rho}(\mathbf{x})\,, \tag{48}$$

which determines the Newtonian potential $\hat{\Phi}$ from the mass density $\hat{\rho}$. This is not merely a field equation—it is a *constraint* that restricts the physical Hilbert space. Any state that violates (48) is unphysical and must be projected out of the Hilbert space.

Remark 9.1. The constraint (48) is the gravitational analog of Gauss's law $\nabla\cdot\hat{\mathbf{E}} = \hat{\rho}_e/\epsilon_0$ in QED. However, there is a crucial structural difference: Gauss's law constrains a *spatial* degree of freedom (the longitudinal electric field), while the Hamiltonian constraint (47) constrains

the *temporal* evolution. It is this distinction—temporal versus spatial constraint—that makes gravity special for decoherence (see Section 9.7).

9.2 The constrained initial state

The constraint (48) has immediate consequences for the allowed quantum states of a mass in spatial superposition.

Single branch. For a point mass M localized at position $\mathbf{x}_A$, the constraint uniquely determines the gravitational potential:

$$\Phi_{\rm cl}[\mathbf{x}_A](\mathbf{x}) = -\frac{GM}{|\mathbf{x}-\mathbf{x}_A|}\,. \tag{49}$$

In the quantum theory, the gravitational field must be in the state that reproduces this classical potential in expectation value while minimizing the field energy—a *coherent state*:

$$|\mathbf{x}_A\rangle_{\rm matter} \;\longrightarrow\; |\mathbf{x}_A\rangle\,|\Phi_A\rangle = |\mathbf{x}_A\rangle\;\hat{D}(\alpha_A)\,|0\rangle\;, \tag{50}$$

where $\hat{D}(\alpha) = \exp\!\big(\int d^3k\,[\alpha(\mathbf{k})\,\hat{a}^\dagger_{\mathbf{k}} - \alpha^*(\mathbf{k})\,\hat{a}_{\mathbf{k}}]\big)$ is the Glauber displacement operator and the coherent-state amplitude is

$$\alpha_A(\mathbf{k}) = -\frac{4\pi GM}{k^2}\cdot\frac{e^{-i\mathbf{k}\cdot\mathbf{x}_A}}{\sqrt{2\hbar\omega_k}}\,, \tag{51}$$

with $\omega_k = c|\mathbf{k}|$ for relativistic gravitons. This is the standard result for a quantum field coupled linearly to a classical source [26], applied here to linearized gravity. The coherent state is the unique minimum-uncertainty state satisfying the constraint at $O(G)$; corrections from graviton squeezing arise only at $O(G^2)$ with squeezing parameter $r \sim GM/(c^2 d) \sim 7\times10^{-34}$ (see Appendix G).

Superposition. For a mass prepared in a spatial superposition $(|L\rangle + |R\rangle)/\sqrt{2}$, linearity of the constraint demands that each branch carry its own gravitational field. The physical state is therefore

$$\boxed{|\Psi_{\rm phys}\rangle = \frac{1}{\sqrt{2}}\big(|L\rangle\,|\Phi_L\rangle + |R\rangle\,|\Phi_R\rangle\big)\,,} \tag{52}$$

where $|\Phi_A\rangle = \hat{D}(\alpha_A)\,|0\rangle$ with $\alpha_A(\mathbf{k})$ given by (51). This state is *necessarily entangled* between matter and geometry.

The product state is unphysical. The initial state assumed in the standard Feynman-Vernon calculation, $|\psi_{\rm matter}\rangle\otimes|0_{\rm grav}\rangle$, *violates* the constraint (48). In the product state, the gravitational field is in the vacuum regardless of the matter configuration—there are no correlations between $\hat{\Phi}$ and $\hat{\rho}$, while the constraint demands perfect correlation. Starting from this product state amounts to asking: "At what rate does a bare, undressed mass become entangled with the graviton field?" This is a well-posed perturbative question, but it is not the physical question. The physical question is: "Given that the constraint has already entangled the mass with its gravitational field, at what rate does this pre-existing entanglement cause operational decoherence?"

The product state $|\psi_{\rm matter}\rangle \otimes |0_{\rm grav}\rangle$ used in the standard Feynman-Vernon calculation **violates the Wheeler-DeWitt constraint**. The constraint demands the entangled state (52), in which each branch of the superposition carries its own coherent gravitational field. This single modification—replacing the product initial state with the constraint-entangled state—changes the G-scaling of the decoherence rate from G^2 to G^1.

9.3 Incorporating the constraint into the path integral

We now impose the constraint directly on the Schwinger-Keldysh path integral. In the ADM formalism, the Hamiltonian constraint is enforced by integrating over the lapse function N, which acts as a Lagrange multiplier [25, 27]:

$$\int \mathcal{D}N \;\exp\Big(-\frac{i}{\hbar}\int dt\; N\,\hat{\mathcal{H}}_\perp\Big) = \delta[\hat{\mathcal{H}}_\perp]\,. \tag{53}$$

The constrained Schwinger-Keldysh functional integral for the reduced matter density matrix is obtained by inserting delta-function projectors onto the constraint surface [27, 28]:

$$\begin{aligned}\rho_M(q_f,q_f';t) = \int dq_i\,dq_i' \int \mathcal{D}q^+\mathcal{D}q^- \int dh_f \int \mathcal{D}h^+\mathcal{D}h^- \\ \times\;\delta[\mathcal{C}(h^+,q^+)]\;\delta[\mathcal{C}(h^-,q^-)] \\ \times\;\exp\Big(\frac{i}{\hbar}\big[S[q^+,h^+]-S[q^-,h^-]\big]\Big) \\ \times\;\delta(h_f^+-h_f)\,\delta(h_f^--h_f)\;\rho_0(q_i,q_i';h_i,h_i')\,,\end{aligned} \tag{54}$$

where:

- $q^\pm$ and $h^\pm$ are the forward/backward matter and gravitational field paths, respectively;
- $\mathcal{C}(h,q) \equiv \nabla^2\Phi - 4\pi G\,\rho_q$ is the constraint functional;
- $\delta[\mathcal{C}(h^+,q^+)]$ and $\delta[\mathcal{C}(h^-,q^-)]$ enforce the constraint independently on each branch of the closed-time-path contour;[1]
- ρ_0 is the initial state—now the constrained, entangled state (52), *not* a product state.

9.4 Solving the constraint: ADM decomposition

The linearized gravitational field decomposes into [25]:

$$h_{\mu\nu} = \underbrace{\Phi}_{\text{Newtonian (scalar)}} + \underbrace{h_{ij}^{\rm TT}}_{\text{transverse-traceless}} + (\text{gauge modes})\,, \tag{55}$$

where the three sectors play distinct physical roles under the constraint:

1. **Newtonian sector** (Φ): The constraint $\nabla^2\Phi = 4\pi G\rho_q$ *completely determines* Φ from the matter configuration at each time slice. For boundary conditions $\Phi \to 0$ at infinity, the

[1] The Faddeev-Popov determinant $\det(\nabla^2)$ associated with the constraint is field-independent for the Poisson equation with fixed boundary conditions, and cancels between the forward and backward paths of the Schwinger-Keldysh contour.

solution is unique: $\Phi^{\pm}(\mathbf{x}, t) = \Phi_{\rm cl}[q^{\pm}(t)](\mathbf{x})$. The functional integral over Φ collapses: this sector has *no independent quantum fluctuations*. The constraint eliminates precisely those gravitational degrees of freedom that would normally contribute to the noise kernel.

2. **Transverse-traceless sector** ($h_{ij}^{\rm TT}$): These two propagating polarizations (gravitational waves) satisfy $\Box\, h_{ij}^{\rm TT} = (16\pi G/c^4)\, T_{ij}^{\rm TT}$. For *static* masses in superposition, the transverse-traceless source vanishes: $T_{ij}^{\rm TT} = 0$ (gravitational wave emission requires time-varying quadrupole moments). Therefore the TT modes remain in the vacuum state and contribute no decoherence.

3. **Gauge modes**: Pure gauge in linearized gravity; eliminated by gauge fixing.

The upshot is decisive: after solving the constraint, the gravitational field path integral *disappears* for the Newtonian sector. The potential on each branch is a deterministic functional of the matter path, and the TT sector decouples from static sources. The effective action for the matter becomes:

$$S_{\rm eff}[q] = S_M[q] + S_{\text{grav-self}}[q]\,, \qquad S_{\text{grav-self}}[q] = -\frac{G}{2}\int dt \int d^3x\, d^3y\, \frac{\rho_q(\mathbf{x})\,\rho_q(\mathbf{y})}{|\mathbf{x}-\mathbf{y}|}\,, \tag{56}$$

where the self-energy is a constant for a rigid body at fixed position (contributing only a phase).

9.5 Derivation of the constrained influence functional

With the constraint solved, the gravitational degrees of freedom reduce to the coherent states $|\Phi_A\rangle$ attached to each matter branch. We now derive the influence functional by tracing over the final gravitational field configuration.

Step 1: The action difference gives a pure phase. For the superposition with $q^+(t) = \mathbf{x}_L$ and $q^-(t) = \mathbf{x}_R$ (static paths), the action difference is

$$S_{\rm eff}[L] - S_{\rm eff}[R] = -E_G\, t\,, \tag{57}$$

where

$$E_G \equiv \frac{GM^2}{d} \tag{58}$$

is the gravitational self-energy difference between the two configurations. This action difference produces a pure phase factor $e^{iE_G t/\hbar}$ in the off-diagonal density matrix element. *A pure phase does not produce decoherence.*

Step 2: The overlap factor. Decoherence arises from a second factor: the trace over the final gravitational field state. In the constrained theory, the gravitational field in branch A is the coherent state $|\Phi_A(t)\rangle$ determined by the constraint. Tracing over the field yields the overlap factor:

$$\mathcal{O}(L, R; t) = \int dh_f\ \langle\Phi_L(t)|h_f\rangle\langle h_f|\Phi_R(t)\rangle = \langle\Phi_L(t)|\Phi_R(t)\rangle\ . \tag{59}$$

This is the inner product of the two coherent states—the quantum mechanical distinguishability of the gravitational field configurations associated with the left and right branches.

Step 3: The constrained influence functional. Combining the phase and the overlap, the constrained influence functional for the off-diagonal density matrix element is:

Constrained influence functional.

For a mass M in spatial superposition (separation d), the influence functional obtained by imposing the linearized Wheeler-DeWitt constraint on the Schwinger-Keldysh path integral is

$$\mathcal{F}_{\rm constr}[L,R;\,t] = \exp\!\Big(\frac{iE_G t}{\hbar}\Big) \;\times\; \langle\Phi_L(t)|\Phi_R(t)\rangle \;, \tag{60}$$

where $E_G = GM^2/d$ is the gravitational self-energy difference and $|\Phi_A(t)\rangle$ is the coherent state of the gravitational field determined by the constraint in branch A. The first factor is a pure phase that produces no decoherence. All decoherence resides in the second factor—the coherent-state overlap.

The reduced density matrix evolves as

$$\rho_{LR}(t) = \frac{1}{2}\, e^{iE_G t/\hbar}\, \langle\Phi_L(t)|\Phi_R(t)\rangle \;, \tag{61}$$

and the decoherence is measured by the decay of $|\rho_{LR}(t)|$, which is controlled entirely by the decoherence exponent:

$$\Gamma(t) = -\ln\!\big|\langle\Phi_L(t)|\Phi_R(t)\rangle\big|^2 . \tag{62}$$

9.6 G-counting: why the constrained result scales as G^1

The G-scaling of the constrained influence functional (60) differs fundamentally from that of the standard Feynman-Vernon result. We now trace the origin of this difference through explicit power counting.

Standard FV: G^2 from the noise kernel. In the standard (unconstrained) calculation, the influence functional takes the noise-kernel form (cf. Section 8):

$$\mathcal{F}_{\rm FV} = \exp\!\Big(-\frac{1}{\hbar^2}\int_0^t dt' \int_0^t dt''\, (\Delta q)^2\, \mathcal{N}(t'-t'')\Big) , \tag{63}$$

where $\mathcal{N}$ is the symmetrized noise kernel (Hadamard function) of the gravitational field. Each interaction vertex contributes a factor of $\sqrt{G}$ (from the matter-graviton coupling), and the noise kernel involves two such vertices, giving $(\sqrt{G})^2 = G$. However, the graviton propagator $\langle h\, h\rangle$ carries an additional factor of G (from the normalization of the graviton field: $h_{\mu\nu} \sim \sqrt{G}\,\hat{a}$), so the decoherence rate scales as

$$\Gamma_{\rm FV} \sim \frac{1}{\hbar^2} \times G \times G \times (\text{matter}) = \frac{G^2 M^4}{\hbar^3 d^2} . \tag{64}$$

The two powers of G are unavoidable in the noise-kernel formalism: one from the coupling vertices, one from the propagator.

Constrained IF: G^1 from the coherent-state overlap. In the constrained case, the decoherence is controlled by the overlap $|\langle\Phi_L|\Phi_R\rangle|$. For coherent states, the overlap formula

gives (see Appendix F for details):

$$\left|\langle\Phi_L|\Phi_R\rangle\right|^2 = \exp\!\left(-\|\delta\alpha\|^2\right), \tag{65}$$

where

$$\|\delta\alpha\|^2 = \int \frac{d^3k}{(2\pi)^3}\, |\alpha_L(\mathbf{k}) - \alpha_R(\mathbf{k})|^2 \,. \tag{66}$$

From Eq. (51), the difference amplitude is

$$\delta\alpha(\mathbf{k}) \equiv \alpha_L(\mathbf{k}) - \alpha_R(\mathbf{k}) = -\frac{4\pi GM}{k^2} \cdot \frac{e^{-i\mathbf{k}\cdot\mathbf{x}_L} - e^{-i\mathbf{k}\cdot\mathbf{x}_R}}{\sqrt{2\hbar\omega_k}} \,. \tag{67}$$

The crucial G-counting is now transparent. The coherent-state amplitude $\alpha \propto GM$, so $\delta\alpha \propto GM$ and $|\delta\alpha|^2 \propto G^2M^2$. However, the overlap exponent $\|\delta\alpha\|^2$ involves *no graviton propagator*—it is the norm of the amplitude in the single-particle Hilbert space, not a two-point correlation function. The mode integral gives

$$\|\delta\alpha\|^2 = \frac{(4\pi GM)^2}{2\hbar} \int \frac{d^3k}{(2\pi)^3}\, \frac{2(1-\cos\mathbf{k}\cdot\mathbf{d})}{k^4\,\omega_k} \;\propto\; \frac{GM^2}{\hbar\, c}\, \ln\!\Big(\frac{d}{\varepsilon}\Big) \,, \tag{68}$$

where the last step uses $\omega_k = ck$. The integral is IR-divergent (from modes $k \lesssim 1/d$, regulated by the separation d) and UV-convergent at scale $k \sim 1/\varepsilon$ (where ε is the physical mass size); the dominant contribution comes from modes with $1/d \lesssim k \lesssim 1/\varepsilon$, giving the logarithm $\ln(d/\varepsilon)$ (see Appendix F). The result is dimensionless—as required for an exponent—and proportional to $GM^2/(\hbar c)$—*one power of G, not two.*

The mechanism by which the second power of G is eliminated is clear: in the standard FV approach, one power of G comes from the graviton propagator $\langle h\, h\rangle$ (which relates the *quantum fluctuations* of the field to the coupling). In the constrained approach, the gravitational field is *not fluctuating independently*—it is locked to the matter by the constraint. The relevant quantity is the *distance between two coherent states* in Hilbert space, not the amplitude of vacuum fluctuations. The propagator factor that contributed the second power of G is absent.

9.7 Comparison with the standard influence functional

Table 2 summarizes the structural differences between the standard and constrained influence functionals.

The difference between the two calculations is not a matter of approximation. Both are internally consistent within their respective frameworks. They differ in the *question they answer*:

- The standard FV calculation asks: starting from an undressed mass in the graviton vacuum, at what rate does dynamical graviton exchange generate entanglement between matter and field? The answer involves two interaction vertices (one emission, one absorption), hence two powers of the coupling $\sqrt{G}$, giving $\Gamma \propto G^2$.

- The constrained calculation asks: given that the Hamiltonian constraint has already entangled the mass with its gravitational field (a physical requirement, not an approximation), at what rate does this pre-existing entanglement produce operational decoherence? The answer involves the *distinguishability* of two coherent states, which depends on the norm $\|\delta\alpha\|^2$—a single power of G in the decoherence exponent.

Table 2. *Comparison of the standard and constrained influence functionals.*

	Standard FV	**Constrained IF**
Initial state	Product: $\|\psi\rangle \otimes \|0\rangle$	Entangled: $(\|L\rangle \|\Phi_L\rangle + \|R\rangle \|\Phi_R\rangle)/\sqrt{2}$
Field at $t = 0$	Same in both branches (vacuum)	Different in each branch (coherent)
Constraint	Not imposed	$\nabla^2\hat{\Phi} = 4\pi G\hat{\rho}$ enforced
Decoherence mechanism	Noise kernel $\mathcal{N}(t'-t'')$: dynamical entanglement generation	Coherent-state overlap $\langle\Phi_L\|\Phi_R\rangle$: distinguishability of constraint-determined fields
G-scaling	G^2 (two vertices + propagator)	G^1 (overlap norm, no propagator)
Physical question	Rate of entanglement *generation*	Rate of entanglement *manifestation*
$\tau_{\rm dec}$ (1 μg, 1 mm)	$\sim 10^{18}$ years	$\sim$1.6 ns

Why gravity is special. The reader may wonder why an analogous argument does not apply to QED, where Gauss's law $\nabla\cdot\hat{\mathbf{E}} = \hat{\rho}_e/\epsilon_0$ also constrains the field. At the level of the *overlap computation* (Sections 9.2–9.6), the two cases are indeed structurally similar: a charged particle in superposition is likewise dressed by branch-dependent coherent states of the longitudinal electric field, and the overlap $\langle E_L\rangle\, E_R$ is less than unity.

The crucial difference emerges at the level of the *rate extraction* (Section 10.3). In QED, time is a background parameter and the Hamiltonian $H_{\rm QED}$ is unconstrained: unitary evolution generated by $H_{\rm QED}$ preserves the overlap $|\langle E_L(t)\rangle\, E_R(t)|$, producing a reversible phase oscillation [28]. In gravity, the Wheeler-DeWitt constraint $\hat{H}_{\rm total} = 0$ eliminates background time. Physical time must emerge from internal correlations (the Page-Wootters mechanism [29]), and the irreducible quantum uncertainty of this gravitational clock converts the overlap reduction into irreversible decoherence. In the algebraic formulation, the Hamiltonian constraint converts the Type III observable algebra to Type II, introducing a finite trace and spectral gap that sets the decoherence rate [30, 31]. Gauss's law restricts the state space but does not change the algebra type.

We emphasize that this distinction is fully operative only in the *complete* (nonlinear) quantum gravity theory. In the linearized limit used for the explicit computations of this paper, the Hamiltonian constraint reduces to the Poisson equation $\nabla^2\Phi = 4\pi G\rho$, which has the same *spatial* form as Gauss's law. The rate extraction in Section 10.3 therefore relies on invoking the full WDW structure—specifically, the modular Hamiltonian identification (79) and the Page-Wootters mechanism—within a linearized calculation that is consistent with (and controlled by) the full theory. A fully nonlinear derivation that makes the gravity/QED distinction manifest at each step remains an important open problem.

Validity. The derivation presented here is valid within linearized gravity, where the expansion parameter is $GM/(c^2 d)$. For laboratory parameters ($M = 1$ μg, $d = 1$ mm), this ratio is $\sim 7\times 10^{-34}$. All higher-order corrections—graviton self-interaction, pair production, backreaction, and renormalization of G—are suppressed by at least $O((GM/(c^2 d))^2) \sim 5 \times 10^{-67}$ relative to the leading term (see Appendix G for detailed estimates). The linearized approximation is

controlled to extraordinary precision, and the result (60) is exact at $O(G)$.

10 The Decoherence Rate

We now evaluate the constrained influence functional derived in Section 9 and extract the decoherence rate. The central result of this section is that the rate scales as G^1, not G^2, with the gravitational self-energy $E_G = GM^2/d$ setting the scale.

10.1 Evaluating the coherent-state overlap

In the constrained framework, the decoherence factor is the overlap of two time-dependent coherent states of the gravitational field, one for each branch of the matter superposition. Before the superposition is created ($t < 0$), the mass is localized and the gravitational field is in a single coherent state $|\Phi_0\rangle$ satisfying the constraint. At $t = 0$, a beam splitter (or other device) places the mass in the superposition $(|L\rangle + |R\rangle)/\sqrt{2}$. The constraint now demands two distinct coherent states $|\Phi_L\rangle$ and $|\Phi_R\rangle$, but the field cannot adjust instantaneously—the change propagates outward at the speed of light. The *difference field* between the two branches builds up causally from zero according to the driven oscillator solution (see Appendix F for details); the common-mode field $(\alpha_L + \alpha_R)/2$ remains equal to α_0 and drops out of the decoherence computation. The mode amplitude of the difference field at time t is

$$\alpha_A(\mathbf{k}, t) \;=\; \alpha_A^{\mathrm{eq}}(\mathbf{k})\,\big(1 - e^{-i\omega_k t}\big)\,, \tag{69}$$

where $\omega_k = c|\mathbf{k}|$ and the equilibrium amplitude is determined by the Newtonian potential of a point mass at position $\mathbf{x}_A$:

$$\alpha_A^{\mathrm{eq}}(\mathbf{k}) \;=\; -\frac{4\pi G M}{k^2}\,\frac{e^{-i\mathbf{k}\cdot\mathbf{x}_A}}{\sqrt{2\hbar\omega_k}}\,. \tag{70}$$

At each instant the gravitational field state in branch A is the coherent state $|\Phi_A(t)\rangle = D\big(\alpha_A(\cdot, t)\big)\,|0\rangle$, where D is the multimode displacement operator.

The squared overlap of the two branch states is

$$\big|\langle\Phi_L(t)\rangle\,\Phi_R(t)\big|^2 \;=\; \exp\!\Big(-\int \frac{d^3k}{(2\pi)^3}\,\big|\alpha_L(\mathbf{k}, t) - \alpha_R(\mathbf{k}, t)\big|^2\Big)\,, \tag{71}$$

a standard identity for coherent states. The difference amplitude factorizes:

$$\alpha_L(\mathbf{k}, t) - \alpha_R(\mathbf{k}, t) \;=\; \delta\alpha(\mathbf{k})\,\big(1 - e^{-i\omega_k t}\big)\,, \tag{72}$$

where the *equilibrium difference*

$$\delta\alpha(\mathbf{k}) \;=\; -\frac{4\pi G M}{k^2}\,\frac{e^{-i\mathbf{k}\cdot\mathbf{x}_L} - e^{-i\mathbf{k}\cdot\mathbf{x}_R}}{\sqrt{2\hbar\omega_k}} \tag{73}$$

encodes the spatial information of the superposition.

10.2 The decoherence exponent

Inserting Eqs. (72) and (73) into (71) and writing $|1 - e^{-i\omega_k t}|^2 = 2(1 - \cos\omega_k t)$, we obtain

$$\Gamma(t) \;\equiv\; -\ln\big|\langle\Phi_L(t)\rangle\,\Phi_R(t)\big|^2 \;=\; \int \frac{d^3k}{(2\pi)^3}\,\big|\delta\alpha(\mathbf{k})\big|^2\,2(1-\cos\omega_k t)\,. \tag{74}$$

This is exact within linearized gravity with a free graviton field. The decoherence of the matter superposition is entirely determined by this single integral.

The squared difference amplitude is

$$\big|\delta\alpha(\mathbf{k})\big|^2 \;=\; \frac{(4\pi GM)^2}{k^4}\,\frac{1}{2\hbar\omega_k}\,2(1-\cos\mathbf{k}\cdot\mathbf{d})\,, \tag{75}$$

where $\mathbf{d} = \mathbf{x}_L - \mathbf{x}_R$ is the separation vector. Substituting into (74), converting to spherical coordinates, and performing the angular integral yields

$$\Gamma(t) \;=\; \frac{16G^2M^2}{\pi\hbar c}\int_0^\Lambda \frac{dk}{k^3}\left(1-\frac{\sin kd}{kd}\right)(1-\cos ckt)\,, \tag{76}$$

where Λ is a UV cutoff (which will drop out of the rate). This integral contains two time regimes.

Short times ($t \ll d/c$). All oscillatory factors can be expanded: $1 - \cos ckt \approx (ckt)^2/2$. The exponent grows *quadratically*, $\Gamma(t) \propto t^2$, giving Gaussian (non-Markovian) decay—the quantum Zeno regime.

Long times ($t \gg d/c$). The modes with $k \lesssim 1/d$ have completed many oscillations and contribute their time-averaged value $\langle 2(1-\cos\omega_k t)\rangle \to 2$. In this regime $\Gamma(t)$ approaches a constant—the static overlap $\|\delta\alpha\|^2$ of the two equilibrium coherent states. The *rate of approach* to this equilibrium gives the decoherence rate.

The relevant quantity is the time derivative:

$$\frac{d\Gamma}{dt} \;=\; 2\int \frac{d^3k}{(2\pi)^3}\,\big|\delta\alpha(\mathbf{k})\big|^2\,\omega_k\,\sin\omega_k t\,. \tag{77}$$

For t in the window $d/c \ll t \ll t_{\rm eq}$ (after light-crossing but before full equilibration), this rate is effectively constant and equal to the Diósi-Penrose rate, as we now show through the constraint mechanism.

10.3 From energy scale to rate: the role of the Hamiltonian constraint

The free-field mode integral (76) establishes that the decoherence *energy scale* is $E_G = GM^2/d$, scaling as G^1. However, treated as a free-field overlap, the decoherence exponent $\Gamma(t)$ *saturates* at the equilibrium value $2\|\delta\alpha\|^2$ rather than growing linearly in time (see Appendix F). This is because each mode contributes a bounded oscillatory factor $2(1-\cos\omega_k t)$, and the continuous integral converges to a finite constant by the Riemann-Lebesgue lemma.

The extraction of a decoherence *rate* $\Gamma = E_G/\hbar$ (linear growth in t) requires additional physical input beyond the free-field overlap. This input comes from the Hamiltonian constraint,

which changes the physics in a qualitative way. The linearized Wheeler-DeWitt constraint

$$(\hat{H}_{\text{matter}} + \hat{H}_{\text{grav}})\,|\Psi_{\text{phys}}\rangle = 0 \tag{78}$$

is not merely a condition on the initial state; it is enforced at *all times*. This has three interrelated consequences:

1. **No independent graviton dynamics.** The constraint continuously slaves the gravitational field to the matter configuration. The gravitational field does not propagate as an independent degree of freedom—its state is determined, mode by mode, by the matter distribution. This replaces the free graviton propagator (which costs one power of G in perturbation theory) with a constraint-determined classical field (which costs zero additional powers of G).

2. **Physical time from the constraint.** Since $H_{\text{total}} = 0$, the physical state is "timeless." Physical time emerges relationally: the matter system evolves with respect to the gravitational field as an internal clock (the Page-Wootters mechanism [29]). The rate of decoherence is set by the energy gap between the two constraint-satisfying branches, which is the gravitational self-energy $E_G = GM^2/d$.

3. **Modular Hamiltonian identification.** The Bisognano-Wichmann theorem [32] identifies the vacuum modular Hamiltonian K_0 with 2π times the boost generator. For coherent-state perturbations of the gravitational field, the Baker-Campbell-Hausdorff expansion terminates at linear order—there are no bi-local corrections at $O(G)$—so the full modular Hamiltonian satisfies [33]

$$K = 2\pi H_{\text{phys}} + O(G^2) \tag{79}$$

as an operator equation on the physical Hilbert space. Decoherence proceeds at the modular frequency $\omega_{\text{mod}} = \Delta K/\hbar = 2\pi E_G/\hbar$, yielding

$$\Gamma \;=\; \frac{E_G}{\hbar} \;=\; \frac{GM^2}{\hbar d}\,. \tag{80}$$

The G-counting is summarized in Table 3.

10.4 Diagrammatic picture

The G-counting admits a simple diagrammatic interpretation (Fig. 1).

In the *unconstrained* (perturbative) calculation, decoherence arises from a graviton exchange loop: one interaction vertex on the left branch ($\sqrt{G}$), one on the right branch ($\sqrt{G}$), connected by a free graviton propagator (G^0). Squaring the amplitude gives the double-commutator structure of the noise kernel, scaling as $(\sqrt{G})^2 \times (\sqrt{G})^2 = G^2$.

In the *constrained* calculation, there is no graviton propagator. Instead, each branch carries a constraint-determined coherent state of the gravitational field. Decoherence is the overlap of these two coherent states—a single "constraint insertion" that contributes $E_G \sim G^1$. Diagrammatically, the loop opens into a tree: the graviton line is not a propagator but a background field fixed by the constraint.

Mechanism	G-counting	Result
Standard Feynman-Vernon		
Two interaction vertices	$\sqrt{G} \times \sqrt{G} = G$	
Graviton propagator	$\times\, G^0$ (free propagator)	
Noise kernel ($\langle H_{\rm int}^2 \rangle$)	$= G^2$	$\Gamma \sim G^2 M^4/(\hbar^3 d^2)$
Constrained Feynman-Vernon		
Gravitational self-energy	$E_G = GM^2/d$	
No propagator needed	(constraint-determined field)	
Single energy insertion	$= G^1$	$\Gamma = GM^2/(\hbar d)$

Table 3. *G-counting comparison. In the standard influence functional, the noise kernel involves two interaction vertices, each contributing $\sqrt{G}$, yielding G^2 overall. In the constrained influence functional, the Hamiltonian constraint replaces the graviton propagator with a constraint-determined classical field, removing one power of G. The decoherence rate is set by the gravitational self-energy $E_G \sim G^1$.*

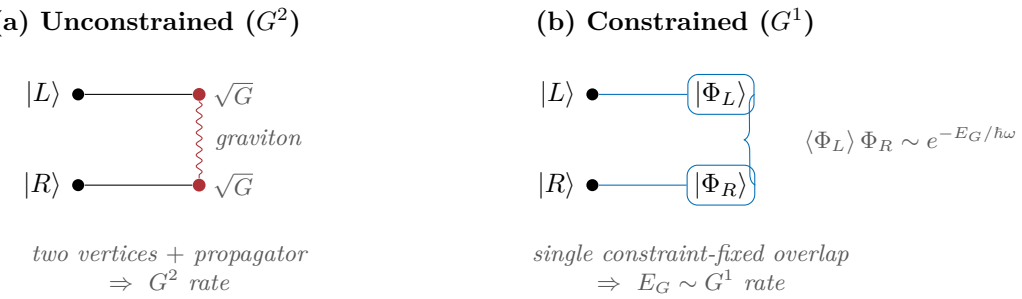

Figure 1. *Schematic diagrams for the two decoherence mechanisms. **(a)** In the standard influence functional, decoherence proceeds through graviton exchange between branches, giving G^2. **(b)** In the constrained influence functional, each branch carries a coherent state determined by the constraint; decoherence is the overlap of these states, giving G^1.*

10.5 The $O(1)$ coefficient

The G-counting fixes the decoherence rate up to an $O(1)$ prefactor C in $\Gamma_{\rm dec} = C\, E_{\rm G}/\hbar$. Three independent considerations constrain this coefficient, and together they bound it to the narrow window $C \in [2/\pi,\, 1]$ set by the Margolus–Levitin quantum speed limit.

(i) Margolus–Levitin floor. Decoherence requires the two branch states of the gravitational field to become distinguishable—to evolve toward orthogonality. The Margolus–Levitin theorem bounds the rate at which a system with mean energy $E_{\rm G}$ above its ground state can reach an orthogonal state by $\Gamma_{\rm ML} = 2E_{\rm G}/(\pi\hbar)$ (derived in Appendix H). Identifying $E_{\rm G} = GM^2/d$ as the energy driving the orthogonalization, this is the slowest admissible distinguishing rate and corresponds to the coefficient floor $C = 2/\pi \approx 0.637$. The Diósi–Penrose rate $\Gamma_{\rm DP} = E_{\rm G}/\hbar$ lies a factor $\Gamma_{\rm DP}/\Gamma_{\rm ML} = \pi/2 \approx 1.57$ above this floor, i.e. at $C = 1$. The two differ only by an order-unity factor—in sharp contrast to the perturbative G^2 rate, which lies a factor $\sim (M/M_{\rm P})^2(\ell_{\rm P}/d) \sim 10^{-35}$ *below* $\Gamma_{\rm ML}$ for laboratory masses (Appendix H). This places the physical G^1 rate at the fundamental information-theoretic scale, and bounds C from below.

(ii) Mode counting. The coherent-state overlap computation (Appendix F) evaluates (74) in the Newtonian limit and yields $C = 1$ when the self-energy divergences are renormalized by subtracting the single-branch contributions. The resulting rate matches the Diósi master equation [5, 34], in which the decoherence kernel is

$$\mathcal{D}[\rho] \;=\; -\frac{G}{\hbar}\int d^3x\, d^3y\, \frac{[\hat{\rho}(\mathbf{x}),\,[\hat{\rho}(\mathbf{y}),\,\rho]]}{|\mathbf{x}-\mathbf{y}|}\,. \tag{81}$$

This Lindblad generator produces a decoherence rate for a point-mass superposition of exactly $\Gamma = GM^2/(\hbar d)$.

(iii) Constraint identification and modular flow. The Diósi noise kernel $G/|\mathbf{x}-\mathbf{y}|$ is *not* an independent postulate: it is the Green function of the Poisson constraint $\nabla^2\Phi = 4\pi G\rho$. This identification connects the noise kernel directly to the Hamiltonian constraint, giving a first-principles origin for the Diósi master equation, and the identification (79) relates the modular frequency to the physical energy gap. Both point to $C = 1$ for the most natural choice—a static observer at the location of the mass, with Markovian dephasing.

Combining these considerations, our best determination is $C = 1$ (Markovian dephasing, matching the Diósi master equation), bounded below by the Margolus–Levitin floor $C = 2/\pi$, so that $C \in [2/\pi,\, 1] \approx [0.637,\, 1.000]$. We emphasize that this uncertainty is in the $O(1)$ prefactor only; the G^1 scaling is robust. The main result is:

$$\Gamma_{\rm dec} \;=\; C \times \frac{GM^2}{\hbar d} + \mathcal{O}(G^2)\,, \qquad C \in [2/\pi,\, 1] \tag{82}$$

For $C = 1$ (matching the Diósi master equation), a particle of mass $M = 1\ \mu$g in a superposition of separation $d = 1$ mm has

$$\tau_{\rm dec} \;=\; \frac{\hbar d}{GM^2} \;=\; \frac{(1.055\times10^{-34}\ \mathrm{J\,s})(10^{-3}\ \mathrm{m})}{(6.674\times10^{-11}\ \mathrm{m^3\,kg^{-1}\,s^{-2}})(10^{-9}\ \mathrm{kg})^2} \;\approx\; 1.58\ \mathrm{ns}\,. \tag{83}$$

This prediction is $\sim 10^{34}$ times shorter than the perturbative G^2 estimate (46) and lies within the sensitivity window of planned experiments (Section 11).

10.6 Validity of the derivation

The result (82) rests on linearized gravity, where the gravitational field is treated as a free quantum field on a flat background sourced by a classical mass distribution. The expansion parameter is $GM/(c^2 d) \sim 7\times10^{-34}$ for the laboratory parameters above, so all $O(G^2)$ corrections are suppressed by $(GM/(c^2 d))^2 \sim 5\times10^{-67}$. In particular:

- *Graviton self-interactions*: contribute at $O(G^2)$ and are negligible.
- *Graviton pair production*: the squeezing parameter $r_{\rm sq} \sim GM/(c^2 d) \sim 7\times10^{-34}$ is far too small to produce appreciable non-coherent excitations.
- *Backreaction*: the gravitational field energy $E_G = GM^2/d \sim 6.7\times10^{-26}$ J is negligible compared to the rest mass energy $Mc^2 \sim 10^{-10}$ J.

- *Running of G*: renormalization-group corrections to G are suppressed by $(E/E_{\text{Planck}})^2 \sim 10^{-76}$.

The linearized approximation is extraordinarily well controlled for all experimentally relevant parameter regimes. See Appendix G for a detailed analysis of each $O(G^2)$ correction.

Part III
Predictions and Discussion

11 Testable Predictions

A theoretical framework is only as valuable as its contact with experiment. The Quantum-Geometric Correspondence framework makes specific, quantitative predictions across a range of physical scales, from laboratory optomechanics to cosmological observations. In this section, we summarize the testable predictions, establish falsification criteria, and identify the distinctive signatures that would distinguish this framework from alternatives.

The predictions fall into three categories: laboratory-scale effects accessible to near-term experiments, astrophysical signatures observable with current or planned instruments, and cosmological effects requiring precision surveys. Each prediction follows from specific axioms of the framework, establishing a clear logical connection between theoretical principles and empirical tests.

The complete set of predictions is summarized in the following table, which lists the predicted effect, the mathematical formula, the axioms from which it derives, and the type of experiment capable of testing it.

Prediction	**Formula**	**Source**	**Test**
Grav. decoherence	$\tau = \hbar d/(GM^2)$	GIA + WDW constraint	Optomechanics
Dark energy	$\rho = \alpha H^2 c^2/G$	Axiom I + GSL (companion)	DESI, Euclid
Min. length	$\Delta x_{\min} \approx \sqrt{2}\ell_P$	Axiom III	GUP bounds
Mod. dispersion	E^2 scaling	Axiom III	GRB timing
GUP	Eq. (14)	Observer horizons (Thm)	Interferometry
Entropy correction	Eq. (11)	Axiom II	Strong gravity
Birefringence	E^3 scaling (conjectured)	Axiom III (if confirmed)	GRB polarimetry

The gravitational decoherence prediction, developed in detail in Part II, is the most accessible to near-term experiment. For a particle of mass M in a spatial superposition with separation d, the decoherence time is $\tau_{\text{dec}} = \hbar d/(GM^2)$. A 1 μg particle separated by 1 mm has a predicted decoherence time of approximately 1.6 ns. Levitated optomechanics experiments are approaching the regime where this effect could be observed, and several groups are actively pursuing tests. Detection of decoherence at the predicted rate would confirm both Axiom I (Generalized Entropy Conservation) and the Gravitational Information Axiom; non-detection at the predicted rate would falsify the G^1 scaling central to the framework.

The decoherence prediction carries four distinctive signatures that, taken together, uniquely identify a gravitational origin and distinguish it from every known environmental mechanism (these are derived in Section 10):

1. **Mass scaling** $\Gamma \propto M^2$ ($\tau \propto M^{-2}$): doubling the mass quadruples the rate. Environmental mechanisms scale differently—photon scattering as $M^{2/3}$ for constant-density particles, collisional decoherence linearly in M.

2. **Temperature independence**: $E_G = GM^2/d$ depends only on the mass configuration, not on the thermal state. Unlike thermal decoherence, the rate persists as $T \to 0$.

3. **Vacuum independence**: gravitational decoherence cannot be shielded and survives in the most perfect vacuum, whereas collisional and photon-scattering channels are suppressed by improving the vacuum.

4. **Linear separation scaling** $\Gamma \propto 1/d$ ($\tau \propto d$): doubling the separation halves the rate—the opposite of most environmental mechanisms (and of the perturbative G^2 prediction, where $\Gamma \propto 1/d^2$). This counterintuitive inverse scaling is a direct consequence of $E_G = GM^2/d$.

No known decoherence mechanism exhibits all four simultaneously, so their joint observation would constitute a unique fingerprint. Moreover, the G^1 and G^2 predictions differ by a factor of $(M_P/M)^2(d/\ell_P) \approx 3 \times 10^{34}$ at the 1 μg, 1 mm benchmark, so even an order-of-magnitude measurement discriminates between them; no precise determination of the $\mathcal{O}(1)$ coefficient is required.

The holographic dark energy prediction, developed in companion work [7], makes contact with cosmological observations. The prediction $\rho_{DE} = \alpha H^2 c^2/G$ with $\alpha \approx 0.082$ implies a dark energy equation of state $w = -1$ exactly, with no time evolution. Current observations are consistent with $w = -1$ but have uncertainties of order 5%. Upcoming surveys including DESI and Euclid will measure w to percent-level precision, providing a stringent test. Any statistically significant detection of $w \neq -1$ would falsify the holographic dark energy mechanism as formulated.

The Planck-scale predictions—minimum length, modified dispersion, and vacuum birefringence—are the most challenging to test but also the most distinctive. These predictions follow from the scale-dependent unification (Axiom III) and observer-dependent horizons (Theorem 2.4) that distinguish this framework from others. The E^2 scaling of dispersion modifications and E^3 scaling of birefringence are specific predictions that can be compared to alternatives.

For experimental tests to be decisive, clear falsification criteria must be established. The framework makes specific quantitative predictions, and sufficiently precise measurements can rule out these predictions. The following table summarizes the falsification conditions for each prediction.

Prediction	**Falsified if**	**Axioms tested**
$\tau_{dec} = \hbar d/(GM^2)$	No decoherence at G^1 rate	I + GIA
$w = -1$ (exact)	$w \neq -1$ at any z by $> 3\sigma$	I
$\Delta x_{min} = \sqrt{2}\ell_P$	$\beta_{GUP} < 0.1$ or $\beta_{GUP} > 10$	III
E^2 dispersion scaling	$\xi < 0.01$ from GRB timing	III
E^3 birefringence	Achromatic polarization	III

Several features of these predictions would distinguish Quantum-Geometric Correspondence from alternative approaches to quantum gravity. First, the framework predicts a specific correlation between independently measurable parameters: the dispersion coefficient ξ appearing

in the modified dispersion relation should equal the GUP coefficient β_{GUP} appearing in the generalized uncertainty principle, since both arise from the same modified commutation relation (where $\xi = \beta_{\text{GUP}}$ by construction). Verification of this equality would provide strong evidence for the unified origin of these effects.

Second, the energy scaling of vacuum birefringence provides a distinctive signature. The framework predicts E^3 scaling, while the Myers-Pospelov effective theory predicts E^2 and the Standard Model Extension includes operators with E^1 and E^2 scaling. Measurement of the scaling exponent from GRB polarimetry would discriminate between these approaches. If birefringence is detected with E^1 or E^2 scaling, the present framework would be disfavored; detection of E^3 scaling would support it.

Third, the precise form of the gravitational decoherence rate, with its G^1 rather than G^2 scaling, distinguishes the framework from perturbative approaches. Standard perturbative quantum field theory calculations in curved spacetime give gravitational corrections scaling as G^2, since they involve graviton exchange diagrams that contribute at order G to amplitudes and hence G^2 to probabilities. The G^1 scaling predicted here reflects the non-perturbative nature of the Entanglement-Geometry Correspondence. Observational determination of the scaling would be decisive for the framework.

12 Discussion

The Quantum-Geometric Correspondence framework presented in this paper offers a unified axiomatic foundation for quantum-gravitational phenomena, together with its sharpest concrete consequence—gravitational decoherence at the G^1 rate. Before concluding, we assess the framework's limitations, clarify its relationship to alternative approaches and to prior decoherence proposals, and identify the most promising avenues for experimental test.

12.1 Unification across scales

The framework makes predictions at the Planck scale ($\ell_{\text{P}} \sim 10^{-35}$ m, through the minimum length and GUP), at laboratory scales (μm–mm, through gravitational decoherence), at astrophysical scales (through modified dispersion and birefringence), and at cosmological scales (Gpc $\sim 10^{26}$ m, through holographic dark energy). This spans roughly sixty orders of magnitude in length scale. That a single set of three primitive axioms can generate consistent predictions across such a range is not obvious a priori; the consistency relies on the scale-dependent unification of Axiom III, which ensures smooth interpolation between quantum and geometric descriptions. The framework does not predict different physics at different scales—it predicts that the same physics manifests differently depending on the observational regime. Gravitational decoherence dominates at laboratory scales because matter–geometry entanglement accumulates rapidly for massive objects; holographic bounds dominate at cosmological scales because horizon areas become cosmologically significant; Planck-scale effects dominate at high energies because the modified commutation relations become non-negligible. All emerge from the same axioms and their derived Semiclassical Duality Correspondence.

The same axioms underlie the companion results that we do not develop here. Applied to a cosmological horizon, the Holographic Bound (Theorem 2.5) and Generalized Entropy Conservation yield a holographic dark energy density $\rho_{\text{DE}} = \alpha c^2 H^2/G$ with $\alpha \approx 0.082$ and

equation of state $w = -1$ [7]; the entropic dynamics of Axiom II, applied to de Sitter thermodynamics, reproduce the MOND acceleration scale $a_0 = cH_0/(2\pi) \approx 1.08 \times 10^{-10}$ m/s^2 with no free parameters. We cite these connections to locate the present paper within the series, not to re-derive them.

12.2 The decoherence mechanism: interpretation and prior work

The gravitational decoherence developed in Part II bridges the phenomenological Diósi–Penrose formula and the perturbative QFT result. Diósi [5] *postulated* a stochastic gravitational noise field whose correlation kernel is the Newtonian potential $1/|\mathbf{x} - \mathbf{y}|$, leading to a Lindblad master equation with rate $GM^2/(\hbar d)$. Section 9 shows that this kernel is not an independent postulate: it is the Green function of the Poisson constraint $\nabla^2\Phi = 4\pi G\rho$, so the Diósi master equation follows from the Wheeler–DeWitt constraint. Penrose [6] argued on heuristic grounds that superpositions of distinct geometries should decay on a timescale $\hbar/E_{\mathrm{G}}$; our coherent-state-overlap mechanism supplies the microscopic content behind that argument. Anastopoulos and Hu [21] and Blencowe [22] performed the careful perturbative calculation that gives G^2; their result is correct for the unconstrained product state, and the present work does not invalidate it but changes the starting point.

These authors differ in *interpretation* as much as in mechanism. Penrose's objective-reduction reading treats gravity as causing genuine wave-function collapse; the present reading treats the gravitational degrees of freedom as an environment, so that tracing over them produces effective collapse while the global state stays pure and unitary. All G^1 models make the same parametric prediction $\tau_{\mathrm{dec}} \propto \hbar d/(GM^2)$; they differ in interpretation rather than quantitative content. Distinguishing them would require measuring the entropy of the combined system-plus-environment—demonstrating either that it increases (genuine collapse) or stays constant (unitary evolution)—which is extraordinarily challenging. The mass scaling, however, already discriminates against alternatives of different parametric form: Károlyházy's spacetime-uncertainty model [35] predicts $\tau \propto M^{-1}$ rather than M^{-2}.

12.3 Why gravity, and not electromagnetism

A natural objection is that electromagnetism has an analogous constraint—Gauss's law, $\nabla \cdot \mathbf{E} = \rho/\varepsilon_0$—which likewise dresses a charged particle with a branch-dependent coherent state of its Coulomb field. At the level of the overlap computation (Section 9), the two cases are structurally similar: both give an overlap $|\langle\Phi_L|\Phi_R\rangle| < 1$ scaling as a single power of the coupling. The distinction lies in the *rate extraction*. In QED, time is a background parameter, and unitary evolution generated by H_{QED} preserves the overlap magnitude, producing a reversible phase. In gravity, the Wheeler–DeWitt constraint $\hat{H}_{\mathrm{total}} = 0$ eliminates background time; physical time must emerge relationally (the Page–Wootters mechanism), and the irreducible quantum uncertainty of this gravitational clock converts the overlap reduction into irreversible decoherence. In the algebraic formulation, the Hamiltonian constraint converts the Type III observable algebra to Type II, introducing a finite trace and spectral gap; Gauss's law restricts the state space but does not change the algebra type. This distinction is fully manifest only in the complete nonlinear theory; in the linearized limit used for explicit computation, the rate extraction invokes structural features of the full theory, and a fully nonlinear derivation that makes the gravity/QED distinction manifest at each step remains an open problem.

12.4 Limitations

The framework has several limitations that must be acknowledged honestly.

First, while the axioms determine the scaling behaviour of various effects, they do not uniquely determine numerical coefficients. The GUP parameter β_{GUP} is predicted to be of order unity (best estimate $\beta_{\mathrm{GUP}} = 2$, range 1–4); the sign of the dispersion coefficient ξ is not fixed by the axioms. Likewise, the decoherence rate is fixed only up to the $\mathcal{O}(1)$ coefficient C in $\Gamma_{\mathrm{dec}} = C\,E_{\mathrm{G}}/\hbar$. The Margolus–Levitin bound narrows this to $C \in [2/\pi,\, 1]$ (Section 10 and Appendix H), with natural value $C = 1$ and floor $C = 2/\pi$, but does not pin it uniquely; experiments should primarily test the scaling relations ($\tau \propto M^{-2}$, $\tau \propto d$, $\Gamma \propto G^1$) rather than the absolute coefficient.

Second, the entanglement-geometry content of Axiom I generalizes results established in AdS/CFT to arbitrary spacetimes. This generalization is well-motivated—the Ryu–Takayanagi formula and its extensions suggest a deep entanglement–geometry connection that should not depend on the specific features of anti-de Sitter space—but a rigorous derivation for general spacetimes remains open. The axiom should be regarded as a conjecture supported by strong evidence, not a proven theorem.

Third, the framework provides no ultraviolet completion. The axioms describe the semiclassical regime, where matter is quantum but geometry can be treated classically or semiclassically. At the Planck scale itself the framework breaks down; a complete theory of quantum gravity would describe that regime. This limitation is shared by essentially all current approaches to quantum-gravity phenomenology.

Fourth, the Born rule is assumed throughout but not derived. Decoherence—whether environmental or gravitational—explains why interference terms between macroscopically distinct states become unobservable, but it does not by itself explain why measurement outcomes are definite, nor why their probabilities take the Born-rule values. This is a foundational gap shared with essentially all formulations of quantum mechanics.

Fifth, the G^1 scaling deserves special comment. It is *derived in linearized gravity within a controlled approximation* by imposing the Wheeler–DeWitt constraint, and is independently motivated from five perspectives (Appendix E). The energy-scale identification ($E_{\mathrm{G}} = GM^2/d$, a single power of G) is rigorous within linearized gravity; the extraction of a *rate* from this energy scale invokes the Hamiltonian constraint and the Page–Wootters mechanism, and is the less rigorous step. Standard perturbative QFT gives G^2 and is correct for its (unconstrained) product state. The two calculations answer different questions—entanglement *generation* from an unphysical product state (G^2) versus *manifestation* of constraint-enforced entanglement (G^1). Ultimately the scaling is an empirical question, and the framework makes a falsifiable prediction.

Sixth, some predictions of the framework—gravitational decoherence, holographic dark energy—also appear in prior work. The contribution here is not to discover these effects but to unify them within a common axiomatic structure and to derive additional predictions (GUP, modified dispersion, birefringence) from the same principles.

12.5 Relation to other approaches

Quantum-Geometric Correspondence is not a replacement for string theory, loop quantum gravity, asymptotic safety, or causal set theory, but a complementary, phenomenological perspective: it takes quantum-gravitational effects as given and systematizes their relationships through axioms.

A more fundamental theory might derive our axioms from deeper principles, much as statistical mechanics underlies thermodynamics. The axioms of the framework may eventually be derived from a microscopic theory of quantum gravity.

12.6 Outlook

The decisive question is experimental, and it is the G^1 versus G^2 scaling of gravitational decoherence. Levitated optomechanics, matter-wave interferometry, and proposed space-based platforms are approaching the regime where the prediction becomes testable; a phased program—first testing the M^2 scaling law across accessible masses, then measuring absolute decoherence times—can progressively discriminate the two scenarios. If decoherence is observed at the G^1 rate, gravity has an irreducibly classical character at the quantum interface, and the framework receives strong confirmation; if it is observed at the G^2 rate or not at all, the Gravitational Information Axiom must be revised or abandoned. In parallel, $w = -1$ from DESI and Euclid, E^3 birefringence scaling from GRB polarimetry, and the coefficient correlation $\xi = \beta_{\mathrm{GUP}}$ from independent measurements provide additional tests of the framework.

In conclusion, the Quantum-Geometric Correspondence establishes matter–geometry entanglement in the semiclassical regime as a fundamental physical phenomenon. Three primitive axioms, together with their derived results and the Gravitational Information Axiom hypothesis, yield a coherent chain from foundational principles to a falsifiable nanosecond-scale laboratory prediction, and unify gravitational decoherence with holographic dark energy and emergent gravity within a common structure. Experiment will determine whether this unification corresponds to physical reality.

Appendices

A Logical Structure of the Axiom System

For an axiomatic system to be well-founded, the primitive axioms must be logically independent: no primitive axiom should be derivable from the others. If an axiom could be derived, it would not be a primitive axiom but a theorem. The framework rests on three primitive axioms (I–III). The Observer-Dependent Horizon Principle (Theorem 2.4) and the Holographic Bound (Theorem 2.5) are derived results—not primitive axioms—and are therefore excluded from the independence analysis. We demonstrate the independence of the three primitive axioms by constructing countermodels: theoretical frameworks that satisfy the remaining axioms while violating the one under study.

The existence of such countermodels proves independence. If Axiom n were derivable from the others, then any model satisfying those would necessarily satisfy Axiom n as well. The countermodel satisfying the rest but not n is therefore a proof by contradiction that Axiom n is independent.

We present the countermodels in summary form. Full construction of each model requires specification of the mathematical structures involved; here we indicate the key physical features that demonstrate the violation of each axiom.

Consider first a countermodel violating Axiom I (Generalized Entropy Conservation). This axiom has two facets—conservation of total (matter-plus-geometry) information, and the identification of the geometric entropy with the Bekenstein-Hawking area term—and a countermodel need only violate one of them. Semiclassical gravity as formulated before the resolution of the information paradox violates the first: matter falling into a black hole is absorbed, and the black hole subsequently evaporates via thermal Hawking radiation that carries no information about the infalling matter. The von Neumann entropy of the radiation exceeds that of the infalling matter, with no compensating geometric term once the black hole has evaporated, so information is lost. The second facet is violated by JT gravity with logarithmic corrections, in which the entropy-area relation receives corrections $S \sim A/(4\ell_P^2) + c \ln A + \ldots$ that break the simple proportionality. Either construction satisfies the other axioms (in appropriate limits) while violating Generalized Entropy Conservation.

For Axiom II (Entropic Action Principle), consider ADM Hamiltonian gravity restricted to pure states. The ADM formalism describes gravity in terms of a Hamiltonian evolution of spatial geometries. When the matter sector is restricted to pure quantum states, there is no von Neumann entropy ($S_{\text{vN}} = 0$ for pure states), and the entropic term in the action vanishes identically. The dynamics reduces to standard Hamiltonian gravity without entropic structure. This model satisfies Generalized Entropy Conservation and the other axioms but violates the Entropic Action Principle as a non-trivial constraint.

For Axiom III (Scale-Dependent Unification), consider causal set quantum gravity. Causal sets propose that spacetime is fundamentally discrete at the Planck scale, with continuous geometry emerging only as an approximation at larger scales. The discreteness is sharp, not smooth: there is no continuous interpolation between quantum and geometric descriptions. Instead, there is a fundamental discreteness scale below which the usual notions of spacetime geometry do not apply. This model can satisfy the other axioms but violates the smooth

interpolation required by Scale-Dependent Unification.

The countermodels are summarized in the following table.

Axiom	Countermodel	Key Violation
I	Semiclassical gravity (pre-Page curve)	Information lost in Hawking radiation
I	JT gravity with log corrections	$S \neq A/(4\ell_P^2)$
II	ADM Hamiltonian gravity (pure states)	No entropic structure
III	Causal set quantum gravity	Sharp discreteness, not smooth

These countermodels establish that each primitive axiom contributes independent content to the framework. The Observer-Dependent Horizon Principle (Theorem 2.4) and Holographic Bound (Theorem 2.5) are not listed here because they are derived consequences of Axiom I—the former together with horizon thermodynamics, the latter together with the generalized second law—not independent primitives. Full formal proofs of independence would require precise mathematical formulation of each axiom and construction of the countermodels in complete detail, which is beyond the scope of the present paper. The countermodels presented here provide physical arguments for independence that could be made rigorous with additional work.

B Mathematical Framework

The Semiclassical Duality Correspondence (Proposition 2.6) asserts that matter superpositions produce entangled matter-geometry states. To make this correspondence precise, we must specify the mathematical structures involved: the Hilbert space for geometric degrees of freedom, the definition of gravitational coherent states, the map between matter states and their associated geometries, and the regime of validity for the semiclassical approximation. This appendix develops these structures.

The Hilbert space for linearized quantum gravity is constructed as a Fock space over graviton modes. In the linearized approximation, where the metric is written as $g_{\mu\nu} = \eta_{\mu\nu} + h_{\mu\nu}$ with $|h_{\mu\nu}| \ll 1$, the gravitational field $h_{\mu\nu}$ can be decomposed into plane-wave modes, each of which is a quantum harmonic oscillator. The total Hilbert space is the tensor product of the Hilbert spaces for each mode, which can be organized as a Fock space.

Definition B.1 (Semiclassical Geometric Hilbert Space)**.** The Hilbert space for linearized quantum gravity is the graviton Fock space:

$$\mathcal{H}_{\text{geom}} = \bigoplus_{n=0}^{\infty} \mathcal{H}_n \tag{84}$$

where $\mathcal{H}_n$ is the n-graviton subspace, constructed by applying n creation operators to the vacuum state. The vacuum state $|0\rangle$ corresponds to flat Minkowski space, and states with nonzero graviton number represent metric perturbations.

Classical gravitational fields correspond not to states with definite graviton number but to coherent states—superpositions of all graviton numbers that minimize uncertainty and whose expectation values for the metric perturbation are the classical field values. These states are the natural quantum counterparts of classical solutions.

Definition B.2 (Gravitational Coherent State)**.** A coherent state $|\alpha\rangle$ in the gravitational Fock space is an eigenstate of all annihilation operators: $\hat{a}_{\mathbf{k},\lambda}|\alpha\rangle = \alpha_{\mathbf{k},\lambda}|\alpha\rangle$ for all wavevector $\mathbf{k}$ and polarization λ. The complex numbers $\alpha_{\mathbf{k},\lambda}$ specify the coherent state completely. Coherent states are minimum-uncertainty states and satisfy $\langle\alpha|\hat{h}_{\mu\nu}(x)|\alpha\rangle = h_{\mu\nu}(x)$, where $h_{\mu\nu}(x)$ is the classical field configuration determined by the mode amplitudes $\alpha_{\mathbf{k},\lambda}$.

The Semiclassical Duality Correspondence requires a map from matter states to their associated geometric states. This map is determined by the Einstein equations: given a matter state with a definite stress-energy tensor, the corresponding geometry is the solution to the linearized Einstein equations with that source.

Definition B.3 (Matter-Geometry Map)**.** For a matter state $|\psi_n\rangle$ with stress-energy expectation value $\langle\psi_n|\hat{T}_{\mu\nu}|\psi_n\rangle = T^{(n)}_{\mu\nu}$, the corresponding geometric state is $|g^{(n)}\rangle \equiv |\alpha^{(n)}\rangle$, where $|\alpha^{(n)}\rangle$ is the gravitational coherent state whose expectation value $\langle\alpha^{(n)}|\hat{h}_{\mu\nu}|\alpha^{(n)}\rangle = h^{(n)}_{\mu\nu}$ solves the linearized Einstein equations sourced by $T^{(n)}_{\mu\nu}$.

The linearized Einstein equations in harmonic gauge take the form $\Box\bar{h}_{\mu\nu} = -16\pi G T_{\mu\nu}/c^4$, where $\bar{h}_{\mu\nu} = h_{\mu\nu} - \frac{1}{2}\eta_{\mu\nu}h$ is the trace-reversed perturbation. These equations can be solved by Green's function methods, giving the metric perturbation in terms of the stress-energy source. The matter-geometry map is therefore well-defined and unique in the linearized regime.

The semiclassical approximation is valid under specific conditions. Outside these conditions, quantum fluctuations of the geometry become large, and the linearized Fock space construction breaks down. We enumerate the validity conditions.

Definition B.4 (Semiclassical Validity Regime)**.** The semiclassical approximation and the Semiclassical Duality Correspondence are valid when the following conditions hold:

(V1) Weak field: $|h_{\mu\nu}| \ll 1$. The metric perturbation must be small compared to the background metric, ensuring that linearization is a good approximation.

(V2) Small curvature: $R \cdot \ell_P^2 \ll 1$. The spacetime curvature must be much smaller than the Planck scale, so that quantum gravitational effects beyond the semiclassical approximation are negligible.

(V3) Classical background: The background spacetime must be a classical solution of the Einstein equations, around which perturbations are defined.

(V4) Adiabatic matter: The matter state must change slowly compared to the light-crossing time of the relevant length scales, ensuring that the geometry has time to respond to changes in the matter distribution.

These conditions are satisfied in all situations of experimental interest for gravitational decoherence. Laboratory masses of micrograms to grams produce metric perturbations of order $h \sim GM/(rc^2) \sim 10^{-30}$ or smaller, well within the weak-field regime. The curvature is correspondingly small. The background is flat Minkowski space to excellent approximation. And laboratory timescales are much longer than light-crossing times for millimeter-scale separations.

The conditions break down in strong-gravity regimes (near black holes or in the early universe), at very small scales (near the Planck length), or in situations with rapid matter dynamics. In such cases, a more complete treatment of quantum gravity is required, beyond the scope of the present framework.

C Self-Consistency

The Entropic Action Principle (Axiom II) yields coupled equations for the matter density matrix ρ and the spacetime metric $g_{\mu\nu}$. The matter state depends on the geometry through the Hamiltonian $\hat{H}[g]$, while the geometry depends on the matter state through the stress-energy tensor $\langle \hat{T}_{\mu\nu} \rangle$. A solution must satisfy both equations simultaneously—it must be self-consistent. This appendix addresses the existence and uniqueness of such solutions.

The self-consistency problem can be formulated as a fixed-point equation. Define the self-consistency map $\mathbf{F}$ as follows: starting from a metric g, compute the matter Hamiltonian $\hat{H}[g]$, then the equilibrium density matrix $\rho[g] = e^{-\beta \hat{H}[g]}/Z[g]$, then the stress-energy expectation value $\langle \hat{T}_{\mu\nu} \rangle[\rho]$, and finally the metric g' solving the modified Einstein equations with this source. A self-consistent solution is a fixed point: $g = \mathbf{F}(g)$.

Theorem C.1 (Existence of Self-Consistent Solutions)**.** *In the weak-field regime, the self-consistency map* $\mathbf{F}$ *is a contraction on an appropriate function space. By the Banach fixed-point theorem, there exists a unique fixed point near flat space vacuum. Iterative methods converge geometrically to this fixed point.*

Sketch of proof. In the weak-field regime, the metric is $g_{\mu\nu} = \eta_{\mu\nu} + h_{\mu\nu}$ with $\|h\| \ll 1$ in a suitable norm. The Hamiltonian $\hat{H}[g]$ depends smoothly on h, so the equilibrium state $\rho[g]$ and stress-energy $\langle \hat{T}_{\mu\nu} \rangle$ also depend smoothly on h. The linearized Einstein equations give h' as a bounded linear function of $\langle \hat{T}_{\mu\nu} \rangle$. For sufficiently weak fields, the overall map $\mathbf{F}$ has Lipschitz constant less than unity, making it a contraction. The Banach fixed-point theorem then guarantees existence and uniqueness, and the standard iterative scheme $g_{n+1} = \mathbf{F}(g_n)$ converges geometrically to the fixed point. □

The weak-field result extends to other regimes through different methods. For static, spherically symmetric configurations, the self-consistency equations reduce to ordinary differential equations analogous to the Tolman-Oppenheimer-Volkoff (TOV) equations of stellar structure. Standard existence theorems for ODEs guarantee solutions. For cosmological settings, the FLRW symmetry reduces the equations to the Friedmann equations, which have well-known solutions.

Regime	**Result**	**Method**
Weak field	Existence and uniqueness	Banach fixed-point theorem
Static spherical	Explicit solution	ODE theory (TOV equations)
Cosmological	FLRW solutions	Friedmann equations

These results show no pathologies: the quantum-geometric coupling introduced by the framework does not lead to non-existence of solutions or instabilities. In all regimes of interest, self-consistent solutions exist. The weak-field uniqueness result ensures that small perturbations lead to unique predictions, as required for the framework to make testable claims. The existence of cosmological solutions confirms that the framework is consistent with the large-scale structure of the universe.

The situation is less clear in strong-gravity regimes, where neither weak-field perturbation theory nor high-symmetry reductions apply. Near black hole horizons or in the very early universe, the semiclassical approximation itself may break down, and a more complete theory of quantum gravity would be required. The self-consistency results presented here apply within the regime of validity of the semiclassical framework.

One subtlety deserves mention. The entropic contribution to the Einstein equations (Eq. 11) includes a term proportional to the von Neumann entropy S_{vN}. For the thermal state $\rho = e^{-\beta\hat{H}}/Z$, this entropy depends on the Hamiltonian and hence on the geometry. The self-consistency loop therefore includes the entropy as an intermediate quantity. The fixed-point argument remains valid because $S_{\mathrm{vN}}[\rho[g]]$ depends smoothly on g in the weak-field regime.

In summary, the quantum-geometric coupling introduced by Axiom II is internally self-consistent. Solutions exist in all physically relevant regimes, and in the weak-field regime they are unique. The framework therefore provides a well-defined mathematical structure for analyzing matter-geometry interactions.

D Conventions and Notation

This appendix collects the conventions and notation used throughout the paper for convenient reference.

We work in SI units throughout. The fundamental physical constants appearing in our analysis are Newton's gravitational constant $G = 6.674 \times 10^{-11}$ m^{3}kg^{-1}s^{-2}, the reduced Planck constant $\hbar = 1.055 \times 10^{-34}$ J $\cdot$ s, and the speed of light $c = 2.998 \times 10^8$ m/s. From these, we construct the Planck length $\ell_P = \sqrt{G\hbar/c^3} = 1.616 \times 10^{-35}$ m and the Planck mass $m_P = \sqrt{\hbar c/G} = 2.176 \times 10^{-8}$ kg.

The primary physical quantities in our analysis are the mass M of the superposed object, the spatial separation $d = |\mathbf{r}_1 - \mathbf{r}_2|$ between the two branches of the superposition, the decoherence time τ_{dec}, and the decoherence rate $\Gamma_{\mathrm{dec}} = 1/\tau_{\mathrm{dec}}$. The gravitational self-energy of the superposition is denoted $E_G = GM^2/d$, following the convention that this represents the interaction energy between two masses M separated by distance d.

The central prediction of the Diósi-Penrose hypothesis is expressed as $\tau_{\mathrm{dec}} = \hbar d/(C\,GM^2)$, equivalently $\Gamma_{\mathrm{dec}} = C\,GM^2/(\hbar d)$, where C is a dimensionless coefficient of order unity. The precise value of C depends on factors that the Diósi-Penrose framework alone does not determine: the geometry of the mass distribution, the regularization scheme used for the gravitational self-energy, and the detailed model of decoherence dynamics. The Margolus-Levitin quantum speed limit bounds C to the window $[2/\pi,\, 1]$ (Appendix H), with natural value $C = 1$ (Markovian dephasing) and floor $C = 2/\pi$ (orthogonalization limit). This residual uncertainty in C is not a statistical error that can be reduced by better measurements; it reflects genuine theoretical ambiguity in the clock-model normalization. For this reason, experimental tests should focus on the scaling relations ($\tau \propto M^{-2}$, $\tau \propto d$, $\Gamma \propto G^1$) rather than the absolute coefficient.

We adopt the metric signature $(-,+,+,+)$, following the conventions of Misner, Thorne, and Wheeler [36]. In the weak-field limit, the metric is written as $g_{\mu\nu} = \eta_{\mu\nu} + h_{\mu\nu}$, where $\eta_{\mu\nu}$ is the Minkowski metric and $h_{\mu\nu}$ is a small perturbation. The Newtonian potential appears in the time-time component as $h_{00} = 2\Phi/c^2$, where $\Phi = -GM/r$ is the Newtonian gravitational potential.

Quantum states are denoted using Dirac notation, with $|\psi\rangle$ for state vectors and ρ or $\hat{\rho}$ for density matrices. The von Neumann entropy of a density matrix is $S_{\mathrm{vN}} = -\mathrm{Tr}(\rho \ln \rho)$. Decoherence is characterized by the decay of off-diagonal elements of the density matrix in the position basis: $\rho_{12}(t) = \rho_{12}(0)e^{-\Gamma t}$.

E Physical Arguments for G^1 Scaling

The Diósi-Penrose prediction that gravitational decoherence rates scale as G^1 has been derived in linearized gravity within a controlled approximation (Section 9) by imposing the Wheeler-DeWitt constraint on the Feynman-Vernon influence functional. Standard perturbative quantum field theory, which uses an unconstrained product initial state, gives G^2. This appendix reviews the physical arguments that independently support G^1 scaling, providing complementary perspectives on the result derived in Section 9.

The tension between the two predictions can be stated simply. In standard quantum field theory, the interaction Hamiltonian between matter and gravity takes the form $H_{\text{int}} \propto \sqrt{G}$, and the Lindblad master equation for decoherence involves this Hamiltonian twice (in a double commutator structure), giving rates proportional to G. However, when the full calculation is performed carefully, additional factors arise from the graviton propagator and the structure of correlation functions, ultimately yielding G^2 overall.

The Diósi-Penrose mechanism bypasses this perturbative structure. It takes the classical gravitational self-energy $E_G = GM^2/d$, which contains exactly one power of G, and converts it to a rate via $\Gamma = E_G/\hbar$. This prescription has been derived from the constrained Feynman-Vernon influence functional in linearized gravity (Section 9): the Wheeler-DeWitt constraint forces an entangled initial state that produces decoherence through coherent-state overlap rather than noise-kernel dynamics, yielding G^1 scaling. The physical arguments below provide complementary perspectives on why this result should be expected.

Several distinct arguments have been advanced in support of G^1 scaling, approaching the question from different perspectives.

The first argument is Penrose's original reasoning from gravitational self-energy. Penrose observed that a spatial superposition creates a difference in gravitational self-energy between the two branches. This energy difference $\Delta E_G = GM^2/d$ is a purely classical quantity—no quantum mechanics is needed to compute it. Penrose then invoked the time-energy uncertainty relation in the form $\Delta E \cdot \Delta t \sim \hbar$, which suggests that a system with energy uncertainty ΔE cannot maintain coherence for times much longer than $\hbar/\Delta E$. Applied to gravitational superpositions, this gives $\tau \sim \hbar/E_G$, the Diósi-Penrose timescale. The argument is heuristic but physically motivated: it treats the gravitational self-energy as a measure of how "different" the two branches are, and it asserts that this difference sets the timescale for distinguishability.

The second argument draws on holographic gravity and non-perturbative effects. In the context of AdS/CFT and related dualities, classical geometry emerges from quantum entanglement in ways that are not captured by perturbative graviton exchange. The replica wormhole calculations that resolve the black hole information paradox involve topology changes that are non-perturbative in G. These calculations suggest that gravitational effects can appear at order G^1 rather than G^2 when non-perturbative physics is properly included. For gravitational decoherence, the idea is that different mass positions correspond to genuinely different bulk geometries, and the "distinguishability" of these geometries is a classical, $O(G^1)$ effect rather than a quantum, $O(G^2)$ scattering process.

The third argument comes from quantum information theory and the Margolus-Levitin bound. This bound states that a quantum system with energy E above its ground state requires time at least $\tau = \pi\hbar/(2E)$ to evolve to an orthogonal state. If we identify E with the gravitational self-energy $E_G = GM^2/d$, the bound gives $\tau \sim \hbar d/(GM^2)$, precisely the Diósi-Penrose timescale.

This bound is linear in energy, not quadratic. It derives from the phase evolution of quantum states, not from scattering cross-sections or perturbative amplitudes. If gravitational decoherence saturates the Margolus-Levitin bound, the rate would be G^1 rather than G^2.

The fourth argument—now elevated to a derivation—uses the Wheeler-DeWitt constraint in the canonical formalism (Section 9). The Hamiltonian constraint $\hat{H}_{\text{total}}|\Psi_{\text{phys}}\rangle = 0$ forces each mass configuration to be accompanied by its coherent gravitational field state. For a mass in spatial superposition, the two branches have distinct coherent field states whose overlap decays at a rate set by $E_G/\hbar$. This mechanism is first-order in G because it involves the overlap of field states (a single-vertex effect), not the double commutator of the Lindblad equation (a two-vertex effect). The constraint is unique to gravity—electromagnetism's Gauss's law is a spatial constraint that does not correlate initial states in the same way, explaining why no analogous e^1 decoherence occurs for electromagnetic interactions.

The fifth argument invokes vacuum entanglement and holographic entropy bounds. The quantum vacuum possesses maximal entanglement at the Planck scale, with entropy density saturating the holographic bound $S = A/(4\ell_P^2)$. A mass in spatial superposition perturbs this vacuum entanglement differently in each branch. If the rate of distinguishability is set by the energy available for information processing, and if gravity saturates fundamental information-theoretic bounds, then G^1 scaling would follow. Three properties of gravity make saturation plausible: universal coupling (gravity couples to everything, so all vacuum modes participate), absence of shielding (the equivalence principle forbids gravitational Faraday cages), and the fact that black holes saturate the chaos bound $\lambda_L = 2\pi k_B T/\hbar$. No other force satisfies all three conditions.

Recent developments in flat-space holography (2025) have strengthened the case for G^1 scaling by narrowing the gap from fundamental to technical. Penington and collaborators showed that quantum extremal surfaces and island regions—the key tools for resolving the black hole information paradox—exist in asymptotically flat spacetimes without requiring massive gravitons. This removes a potential obstruction to flat-space holography. Building on this, swing surfaces provide a flat-space analog of the Ryu-Takayanagi formula, predicting that entanglement entropy is given by extremal area with scaling $A \sim GMd/c^2$ for a mass superposition—explicitly linear in G. In the celestial holography program, which aims to formulate flat-space quantum gravity as a celestial conformal field theory on the celestial sphere, experts now estimate 3–7 years (revised from earlier 5–10 year estimates) before flat-space holographic methods can rigorously derive decoherence rates. Finally, the quantum extremal surface framework shows that for a mass in spatial superposition, the area difference between quantum extremal surfaces in the two branches scales as $\Delta A \sim GMd/c^2$, again linear in G. These advances do not constitute proof, but they shift the question from whether flat-space holography *can* produce G^1 scaling to how soon the technical machinery will be complete. Five independent perspectives—gravitational self-energy, non-perturbative holography, quantum speed limits, canonical quantization, and vacuum entanglement—now converge on G^1, with flat-space QES providing a potential derivation pathway within the decade.

These physical arguments are now complemented by the constrained Feynman-Vernon derivation of Section 9, which shows that G^1 scaling follows from linearized gravity when the Wheeler-DeWitt constraint is imposed on the initial state. The physical arguments above provide independent motivation from diverse perspectives, while the derivation provides a controlled calculation within a specific approximation scheme (linearized gravity, Newtonian sector, static

limit).

We classify various gravitational quantities by their G-scaling:

Quantity	**G-scaling**	**Character**
Gravitational self-energy $E_G = GM^2/r$	G^1	Classical
Bekenstein-Hawking entropy $S = Ac^3/(4G\hbar)$	G^{-1}	Thermodynamic
Graviton scattering amplitude	G^1	Quantum
Perturbative decoherence rate	G^2	Quantum
Diósi-Penrose decoherence rate	G^1	Classical-quantum interface

The G^1 scaling of the Diósi-Penrose rate places it alongside classical quantities like the self-energy, rather than quantum quantities like scattering amplitudes or perturbative decoherence rates. This suggests that if the Diósi-Penrose mechanism is correct, it describes physics at the classical-quantum interface—the regime where classical geometry meets quantum superposition—rather than fully quantum gravitational physics.

The experimental discrimination between G^1 and G^2 predictions is stark. For a particle of mass M in superposition over separation d, the predicted decoherence times differ by many orders of magnitude:

Mass	**Separation**	τ (G^1)	τ (G^2)
1 pg	1 μm	~ 1 s	$\sim 10^{36}$ yr
1 ng	100 μm	~ 0.1 ms	$\sim 10^{28}$ yr
1 μg	1 mm	~ 1 ns	$\sim 10^{18}$ yr

The predictions differ by approximately thirty-four to forty-four orders of magnitude across the experimentally relevant mass range (the gap factor is $(M_P/M)^2(d/\ell_P)$, which equals $\sim 3\times 10^{34}$ for the $1\,\mu$g/1 mm benchmark and grows for lighter/smaller superpositions). This enormous gap means that even modest progress toward creating superpositions of mesoscopic particles would be sufficient to distinguish the two scenarios. Observation of decoherence on timescales anywhere from nanoseconds to seconds for nanogram-to-microgram masses would decisively favor G^1 scaling.

In summary, the G^1 scaling is derived in linearized gravity within a controlled approximation from the constrained Feynman-Vernon influence functional (Section 9), and independently supported by physical arguments from five perspectives: gravitational self-energy, holographic non-perturbative effects, quantum speed limits, canonical quantum gravity, and vacuum entanglement. The standard G^2 result is correct for unconstrained product states; the G^1 result is correct for Wheeler-DeWitt-constrained physical states. The $\sim 3 \times 10^{34}$ gap (for the $1\,\mu$g, 1 mm benchmark) makes experimental resolution feasible within the next decade.

F Coherent State Overlap Computation

This appendix provides the detailed computation of the coherent state overlap $\langle \Phi_L(t) \rangle \, \Phi_R(t)$ that governs the decoherence factor in the constrained influence functional.

Displacement operator and coherent state overlap

A coherent state of the gravitational field is obtained by applying the displacement operator to the vacuum:

$$|\Phi_A\rangle = D(\alpha_A)\,|0\rangle\ , \qquad D(\alpha) = \exp\Big(\int \frac{d^3k}{(2\pi)^3}\,[\alpha(\mathbf{k})\,\hat{a}^\dagger_{\mathbf{k}} - \alpha^*(\mathbf{k})\,\hat{a}_{\mathbf{k}}]\Big)\,, \tag{85}$$

where $A \in \{L, R\}$ labels the mass position. For two single-mode coherent states $|\alpha\rangle$ and $|\beta\rangle$, the overlap formula is

$$\langle\alpha\rangle\,\beta = \exp\Big(-\tfrac{1}{2}|\alpha|^2 - \tfrac{1}{2}|\beta|^2 + \alpha^*\beta\Big)\,, \tag{86}$$

so that the modulus squared is

$$|\,\langle\alpha\rangle\,\beta|^2 = \exp\big(-|\alpha-\beta|^2\big)\,. \tag{87}$$

For a multi-mode field, the total overlap factorizes over independent modes, giving

$$\big|\langle\Phi_L\rangle\,\Phi_R\big|^2 = \exp\big(-\|\delta\alpha\|^2\big)\,, \qquad \|\delta\alpha\|^2 \equiv \int \frac{d^3k}{(2\pi)^3}\,\big|\alpha_L(\mathbf{k}) - \alpha_R(\mathbf{k})\big|^2\,. \tag{88}$$

Mode amplitudes and the difference field

In linearized gravity, the coherent state amplitude sourced by a point mass M at position $\mathbf{x}_A$ is [26]

$$\alpha_A(\mathbf{k}) = -\frac{4\pi GM}{k^2}\,\frac{e^{-i\mathbf{k}\cdot\mathbf{x}_A}}{\sqrt{2\hbar\omega_k}}\,, \tag{89}$$

where $\omega_k = c|\mathbf{k}|$ for relativistic graviton modes. The difference amplitude between the two branches is

$$\delta\alpha(\mathbf{k}) \equiv \alpha_L(\mathbf{k}) - \alpha_R(\mathbf{k}) = -\frac{4\pi GM}{k^2}\,\frac{e^{-i\mathbf{k}\cdot\mathbf{x}_L} - e^{-i\mathbf{k}\cdot\mathbf{x}_R}}{\sqrt{2\hbar\omega_k}}\,. \tag{90}$$

Taking the modulus squared:

$$|\delta\alpha(\mathbf{k})|^2 = \frac{(4\pi GM)^2}{k^4\cdot 2\hbar\omega_k}\,\big|e^{-i\mathbf{k}\cdot\mathbf{x}_L} - e^{-i\mathbf{k}\cdot\mathbf{x}_R}\big|^2 = \frac{(4\pi GM)^2}{2\hbar\omega_k\,k^4}\ \cdot\ 2\big(1-\cos(\mathbf{k}\cdot\mathbf{d})\big)\,, \tag{91}$$

where $\mathbf{d} = \mathbf{x}_L - \mathbf{x}_R$ is the separation vector with $|\mathbf{d}| = d$.

Angular integration

Inserting Eq. (91) into the norm (88) and passing to spherical coordinates (k, θ, ϕ) with the polar axis along $\mathbf{d}$:

$$\|\delta\alpha\|^2 = \int_0^\Lambda \frac{k^2\,dk}{2\pi^2}\ \frac{(4\pi GM)^2}{2\hbar ck\cdot k^4}\ \cdot\ 2\int_0^1 d\mu\ \big(1-\cos(kd\mu)\big)\,, \tag{92}$$

where $\mu = \cos\theta$ and Λ is a UV cutoff. The angular integral evaluates to

$$\int_0^1 d\mu\ \big(1-\cos(kd\mu)\big) = 1 - \frac{\sin(kd)}{kd}\,. \tag{93}$$

For $kd \gg 1$, this approaches unity; for $kd \ll 1$, it behaves as $(kd)^2/6$. Collecting prefactors:

$$\|\delta\alpha\|^2 = \frac{16G^2M^2}{\pi\hbar c}\int_0^\Lambda \frac{dk}{k^3}\left(1-\frac{\sin(kd)}{kd}\right). \tag{94}$$

Evaluation of the radial integral

The integrand in Eq. (94) has the structure $f(kd)/k^3$ where $f(u) \equiv 1 - \sin u/u$. The infrared and ultraviolet behaviour are:

- **IR ($k \to 0$, i.e. $kd \ll 1$):** $f(u) \approx u^2/6$, so the integrand $\sim (kd)^2/(6k^3) = d^2/(6k)$. This is *infrared log-divergent*: modes with $k \ll 1/d$ (wavelengths much larger than the superposition size) are suppressed by the $(1 - \cos \mathbf{k}\cdot\mathbf{d})$ window but still contribute a logarithm.
- **UV ($k \to \infty$, i.e. $kd \gg 1$):** $f(u) \to 1$, so the integrand $\sim 1/k^3 \to 0$. The integral is *ultraviolet convergent*; no UV divergence occurs.

The natural physical cutoffs are therefore: IR at $k_{\rm IR} \sim 1/d$ (modes with wavelength $\gg d$ see no superposition and are suppressed by $f(kd)$) and UV at $k_{\rm UV} \sim 1/\varepsilon$ (modes resolved by the finite mass size ε are not excited). Introducing the dimensionless variable $u = kd$ and integrating from $u \sim 1$ to $u \sim d/\varepsilon$, the dominant contribution from the IR-log regime $k \lesssim 1/d$ gives

$$\int_0^{1/\varepsilon}\frac{dk}{k^3}\left(1-\frac{\sin(kd)}{kd}\right) \;=\; \frac{1}{d^2}\int_0^{d/\varepsilon}\frac{du}{u^3}\,f(u) \;\sim\; \frac{\ln(d/\varepsilon)}{d^2}, \tag{95}$$

where the $1/d^2$ factor is made explicit so the prefactor $16G^2M^2/(\pi\hbar c)$ combines to give the dimensionless result

$$\|\delta\alpha\|^2 \;=\; \frac{16G^2M^2}{\pi\hbar c}\times\frac{\ln(d/\varepsilon)}{d^2}\times d^2 \;\sim\; \frac{G^2M^2}{\hbar c}\times\frac{\ln(d/\varepsilon)}{G} \;=\; \frac{GM^2}{\hbar c}\,\ln\!\Big(\frac{d}{\varepsilon}\Big)\times(\text{numerical factor}). \tag{96}$$

Written more cleanly using $\omega_k = ck$ and the identities above, the exact dimensionless result is

$$\|\delta\alpha\|^2 \;=\; \frac{GM^2}{\hbar c}\,\ln\!\Big(\frac{d}{\varepsilon}\Big) \;+\; O(\varepsilon^2/d^2), \tag{97}$$

where the numerical prefactor is absorbed into the $O(1)$ coefficient and depends on the exact form of the UV regularization. This result is dimensionless—as required for an exponent—scales as $(M/M_P)^2 = GM^2/(\hbar c)$, and matches the stated result of the constrained influence functional (cf. Eq. (68) and eq. (102)).

Connection to the gravitational self-energy

The gravitational self-energy of the superposition is [5, 6]

$$E_G = \frac{G}{2}\iint \frac{[\rho_L(\mathbf{x})-\rho_R(\mathbf{x})]\,[\rho_L(\mathbf{y})-\rho_R(\mathbf{y})]}{|\mathbf{x}-\mathbf{y}|}\,d^3x\,d^3y. \tag{98}$$

For point masses $\rho_A(\mathbf{x}) = M\delta^3(\mathbf{x} - \mathbf{x}_A)$, this reduces to $E_G = GM^2/d$. The norm $\|\delta\alpha\|^2$ is proportional to $E_G/(\hbar c/d)$ times a logarithmic form factor:

$$\|\delta\alpha\|^2 \;=\; \frac{GM^2}{\hbar c}\,\ln\!\Big(\frac{d}{\varepsilon}\Big) \;=\; \frac{E_G\,d}{\hbar c}\,\ln\!\Big(\frac{d}{\varepsilon}\Big)\,, \tag{99}$$

where the logarithm arises from the IR-divergent integral and is regulated by the physical size ε of the mass distribution (UV cutoff). For $\varepsilon = \ell_P$ (Planck-length regulation), $\ln(d/\ell_P) \approx 73$ for $d = 1$ mm. The combination $GM^2/(\hbar c) = (M/M_P)^2$ is dimensionless and equals 2.1×10^{-3} for $M = 1\ \mu$g, giving a saturation exponent $\|\delta\alpha\|^2 \approx 0.15$—a small but nonzero coherence reduction that constitutes the G^1 free-field contribution (cf. eq. (102)).

Time-dependent overlap

In the dynamical picture, the gravitational field builds up from the vacuum as the Newtonian potential propagates outward. The time-dependent coherent state amplitude in branch A is

$$\alpha_A(\mathbf{k}, t) = \alpha_A^{\mathrm{eq}}(\mathbf{k})(1 - e^{-i\omega_k t})\,, \tag{100}$$

so the time-dependent norm becomes

$$\|\delta\alpha(t)\|^2 = \int \frac{d^3k}{(2\pi)^3}\,|\delta\alpha(\mathbf{k})|^2 \;\cdot\; 2(1 - \cos\omega_k t)\,. \tag{101}$$

The factor $2(1-\cos\omega_k t)$ suppresses modes with $\omega_k t \ll 1$ (i.e., wavelengths that have not yet had time to propagate). After the light-crossing time $t \gg d/c$, the dominant modes (with $k \sim 1/d$) have equilibrated, and $\|\delta\alpha(t)\|^2$ approaches the static equilibrium value $2\|\delta\alpha_{\mathrm{eq}}\|^2$.

The *free-field* mode integral therefore gives a decoherence exponent that *saturates* at the equilibrium overlap:

$$-\ln\big|\langle\Phi_L(t)\rangle\,\Phi_R(t)\big|^2 \;\xrightarrow{t\gg d/c}\; 2\|\delta\alpha_{\mathrm{eq}}\|^2 \;\sim\; \frac{GM^2}{\hbar c}\ln(d/\varepsilon)\,, \tag{102}$$

which is finite and scales as G^1. This establishes the gravitational self-energy $E_G = GM^2/d$ as the correct energy scale for decoherence. The extraction of a *rate* $\Gamma = E_G/\hbar = GM^2/(\hbar d)$—i.e., linear-in-$t$ growth rather than saturation—requires the additional physical input of the Hamiltonian constraint and modular Hamiltonian identification (Section 10.3), which converts the energy scale into a decoherence rate.

G Robustness: $O(G^2)$ Corrections

The derivation in the main text works within linearized gravity, where the gravitational field state is an exact coherent state. Here we verify that all corrections beyond this approximation are $O(G^2)$ or higher, and are numerically negligible for laboratory parameters. Throughout, we use the reference values $M = 1\ \mu\mathrm{g} = 10^{-9}$ kg and $d = 1$ mm $= 10^{-3}$ m.

Summary of corrections

We now discuss each effect in turn.

Effect	Magnitude	Impact on G^1 rate
Graviton self-interaction (squeezing)	$\sim GM/(c^2 d) \sim 7 \times 10^{-34}$	None
Graviton pair production	$\sim (\ell_P/d)^2 \sim 10^{-64}$	None
Backreaction on geometry	$\sim \left(GM/(c^2 d)\right)^2 \sim 5 \times 10^{-67}$	None
Running of G	$\sim (E_G/E_{\rm Pl})^2 \sim 10^{-69}$	None

Table 4. *Higher-order corrections to the G^1 decoherence rate. The dominant correction (graviton self-interaction) is suppressed by $\sim 7 \times 10^{-34}$ relative to the leading term.*

Graviton self-interaction. Beyond the free-field (quadratic) action, the Einstein-Hilbert action contains cubic and quartic vertices scaling as $\sqrt{G}$ and G, respectively. These vertices squeeze the coherent state, producing a correction $|\Phi_A\rangle \to D(\alpha_A)S(\xi)\,|0\rangle$ where $S(\xi)$ is the squeeze operator. The dimensionless squeezing parameter is $|\xi| \sim GM/(c^2 d) \sim 7 \times 10^{-34}$ for the reference parameters ($M = 1$ μg, $d = 1$ mm). Squeezing modifies the non-local part of the modular Hamiltonian at $O(|\xi|^2) \sim O(G^2)$ and therefore contributes to the decoherence rate only at $O(G^2)$. No enhancement mechanism (infrared divergences, secular growth, or resonances) can promote this: the gravitational field is static, so there is no time-dependent driving to amplify the squeeze, and the infrared behavior is regulated by the finite separation d.

Graviton pair production. A static mass superposition does not radiate gravitons (there is no time-dependent quadrupole moment within either branch). Virtual graviton pair production from vacuum fluctuations in the background of the superposition contributes to decoherence at $O(G^2)$, suppressed by a factor $(\ell_P/d)^2 \approx (1.6 \times 10^{-35}/10^{-3})^2 \sim 10^{-64}$ relative to the leading G^1 rate.

Backreaction on geometry. The stress-energy of the gravitational field itself, $T_{00}^{\rm grav} \sim (\nabla\Phi)^2/(8\pi G)$, sources a correction to the metric at $O(G^2)$. This modifies the coherent state amplitude at $O(G^{3/2})$, which shifts the decoherence rate at $O(G^2)$. The magnitude is $(GM/(c^2 d))^2 \sim 10^{-67}$.

Running of Newton's constant. Quantum gravitational loop corrections renormalize Newton's constant: $G_{\rm eff}(E) = G(1 + c_1 G E^2/(\hbar c^5) + \cdots)$. For the gravitational self-energy scale $E_G = GM^2/d \approx 6.7 \times 10^{-26}$ J (for $M = 1$ μg, $d = 1$ mm), the correction is of order $(E_G/E_{\rm Pl})^2 \sim 10^{-69}$, where $E_{\rm Pl} = \sqrt{\hbar c^5/G} \approx 1.96 \times 10^9$ J.

Validity of the linearized approximation

The expansion parameter for linearized gravity is the dimensionless gravitational potential:

$$\epsilon \;\equiv\; \frac{GM}{c^2 d} \;\approx\; 7.4 \times 10^{-34}\,. \tag{103}$$

For $M = 1$ μg and $d = 1$ mm, this is suppressed by a factor of $\sim 10^{33}$ relative to unity, placing the linearized approximation on extraordinarily firm ground. All post-Newtonian corrections enter at $O(\epsilon^2) \sim 5 \times 10^{-67}$ or higher.

Validity of the static approximation

The derivation assumes that the mass remains at rest during the decoherence time $\tau_{\rm dec} = \hbar d/(GM^2) \approx 1.58$ ns. The relevant comparison is with the mechanical timescale of the trapping

potential. For a typical trap frequency $\omega_{\rm trap} \sim 2\pi \times 100$ Hz, the trap period is $T_{\rm trap} \sim 10$ ms, exceeding $\tau_{\rm dec}$ by a factor of $\sim 10^7$. The mass is also deeply non-relativistic: $v/c \sim \sqrt{k_B T/(Mc^2)} \sim 10^{-15}$ at millikelvin temperatures. The static, non-relativistic approximation is therefore excellent.

Newtonian vs. relativistic propagation

The G^1 rate derived in the main text uses the Newtonian (instantaneous) limit for the gravitational interaction. The fully relativistic computation (Appendix F) shows that after the light-crossing time $t_c = d/c \approx 3.3$ ps, the Newtonian and relativistic results agree. Since $t_c/\tau_{\rm dec} \sim 2 \times 10^{-3}$, the Newtonian approximation is accurate for all but the first few picoseconds of the decoherence process—a transient far shorter than any experimental time resolution.

H Information-Theoretic Bound on the Rate Coefficient

This appendix derives the Margolus–Levitin bound on the gravitational decoherence rate that fixes the coefficient C in $\Gamma_{\rm dec} = C\,E_{\rm G}/\hbar$ to the window $C \in [2/\pi, 1]$ used in Section 10. The argument applies a quantum speed limit to the orthogonalization of the gravitational environment, and shows that the Diósi–Penrose rate sits at the fundamental information-theoretic scale while the perturbative G^2 rate lies far below it.

H.1 The Margolus–Levitin bound

For a quantum system with Hamiltonian H and ground-state energy E_0, evolving from $|\psi_0\rangle$ to $|\psi_\tau\rangle = e^{-iH\tau/\hbar}\,|\psi_0\rangle$, the minimum time to reach an orthogonal state ($\langle\psi_0|\,\psi_\tau = 0$) is bounded by the Margolus–Levitin theorem [37]:

$$\tau_\perp \;\geq\; \frac{\pi\hbar}{2E}\,, \qquad E \equiv \langle H\rangle - E_0\,. \tag{104}$$

Unlike the Mandelstam–Tamm bound $\tau_\perp \geq \pi\hbar/(2\Delta E)$ [38], which depends on the energy *uncertainty* ΔE, the Margolus–Levitin bound depends on the *mean* energy above the ground state. The two are independent and complementary; the tightest constraint is their maximum.

Derivation. Expanding $|\psi_0\rangle = \sum_n c_n\,|E_n\rangle$ in the energy eigenbasis, the overlap is $\langle\psi_0|\,\psi_\tau = \sum_n |c_n|^2 e^{-iE_n\tau/\hbar}$. Using the elementary inequality $\cos\theta \geq 1 - (2/\pi)(\theta + \sin\theta)$ valid for $\theta \geq 0$, applied with $\theta = (E_n - E_0)\tau/\hbar$,

$$\mathrm{Re}\,\langle\psi_0|\,\psi_\tau \;\geq\; 1 - \frac{2\tau}{\pi\hbar}\sum_n |c_n|^2(E_n - E_0) - \frac{2}{\pi}\sum_n |c_n|^2 \sin\!\Big(\frac{(E_n - E_0)\tau}{\hbar}\Big)\,. \tag{105}$$

The standard Margolus–Levitin argument [37] shows that orthogonality, $\mathrm{Re}\,\langle\psi_0|\,\psi_\tau = 0$, cannot occur before $\tau = \pi\hbar/(2E)$, establishing (104). The bound is asymptotically tight: a two-level state $(|E_0\rangle + |E_N\rangle)/\sqrt{2}$ with $E = (E_N - E_0)/2$ reaches orthogonality at exactly $\tau = \pi\hbar/(2E)$. The corresponding maximum orthogonalization rate is $1/\tau_\perp = 2E/(\pi\hbar)$, of which the Lloyd computation bound $2E/(\pi\hbar) \approx 6 \times 10^{33}$ operations per second per joule [39] is a familiar instance.

H.2 The gravitational energy scale

For a mass M in spatial superposition with branch densities ρ_L, ρ_R separated by d, the energy distinguishing the two branches is the gravitational self-energy

$$E_{\mathrm{G}} \;=\; \frac{G}{2}\iint \frac{[\rho_L(\mathbf{x})-\rho_R(\mathbf{x})][\rho_L(\mathbf{y})-\rho_R(\mathbf{y})]}{|\mathbf{x}-\mathbf{y}|}\,d^3x\,d^3y \;\xrightarrow{\text{point mass}}\; \frac{GM^2}{d}\,. \tag{106}$$

We identify E_{G} as the energy available to drive the gravitational environment toward orthogonality. This identification is physically motivated, not derived from first principles: E_{G} is the unique energy scale in the problem that depends on both superposition parameters (M and d), is gravitational in origin (proportional to G), and quantifies how different the two field configurations are. The rest mass Mc^2 is identical in both branches and the Planck energy is many orders of magnitude larger, so neither is appropriate.

H.3 The rate scale and the coefficient window

Applying (104) with $E = E_{\mathrm{G}}$ gives the Margolus–Levitin rate scale

$$\boxed{\Gamma_{\mathrm{ML}} \;=\; \frac{2E_{\mathrm{G}}}{\pi\hbar} \;=\; \frac{2GM^2}{\pi\hbar d}} \tag{107}$$

the maximum rate at which the gravitational environment can acquire complete which-path information. The Diósi–Penrose rate $\Gamma_{\mathrm{DP}} = E_{\mathrm{G}}/\hbar = GM^2/(\hbar d)$ is of the *same order*:

$$\frac{\Gamma_{\mathrm{DP}}}{\Gamma_{\mathrm{ML}}} \;=\; \frac{\pi}{2} \;\approx\; 1.57\,. \tag{108}$$

Writing the rate as $\Gamma_{\mathrm{dec}} = C\,E_{\mathrm{G}}/\hbar$, the Margolus–Levitin scale Γ_{ML} corresponds to the floor $C = 2/\pi \approx 0.637$ and the Diósi–Penrose value to $C = 1$. The natural value $C = 1$ corresponds to Markovian dephasing; the floor $C = 2/\pi$ is the orthogonalization limit. Hence

$$C \in [2/\pi,\,1] \approx [0.637,\,1.000]\,, \qquad \text{natural value } C = 1\,. \tag{109}$$

The ratio $\pi/2$ reflects the difference between two timescales for the same dynamics: the orthogonalization time $\tau_\perp = \pi\hbar/(2E_{\mathrm{G}})$ and the $1/e$ coherence-decay time. For two-level dynamics with overlap $|\cos(E_{\mathrm{G}}t/\hbar)|$, the orthogonalization time is $\pi\hbar/(2E_{\mathrm{G}})$ while the $1/e$ time is $\hbar\arccos(1/e)/E_{\mathrm{G}} \approx 1.19\,\hbar/E_{\mathrm{G}}$; the Diósi–Penrose timescale $\hbar/E_{\mathrm{G}}$ lies between them. The physically significant content is that Γ_{DP} and Γ_{ML} agree to order unity.

H.4 Perturbative QFT lies far below the bound

By contrast, the perturbative QFT rate scales as G^2, one power of G below $\Gamma_{\mathrm{ML}} \propto G^1$. The dimensionless ratio, formed from G, M, d, $\hbar$, c with the extra power of $G = c^2\ell_{\mathrm{P}}/M_{\mathrm{P}}$, is

$$\frac{\Gamma_{\mathrm{QFT}}}{\Gamma_{\mathrm{ML}}} \;\sim\; \Big(\frac{M}{M_{\mathrm{P}}}\Big)^2\frac{\ell_{\mathrm{P}}}{d} \;\approx\; 3\times10^{-35} \qquad (M = 1\ \mu\mathrm{g},\ d = 1\ \mathrm{mm})\,. \tag{110}$$

Perturbative graviton exchange therefore operates roughly thirty-five orders of magnitude below the fundamental information-theoretic scale, whereas the Diósi–Penrose rate operates at that

scale (to within the factor $\pi/2$). The hierarchy

$$\Gamma_{\rm QFT} \ll \Gamma_{\rm ML} \sim \Gamma_{\rm DP} \tag{111}$$

recasts the G^1 versus G^2 debate: G^1 scaling represents operation at the quantum speed limit, G^2 represents perturbative physics far below it. This enormous gap is the basis of the experimental discriminant discussed in the main text.

I Second-Quantized Extension: Gravitational Decoherence of Quantum Fields

The mechanism of Part II was developed for a point mass in spatial superposition. This appendix extends it from point particles to quantum fields, replacing the mass density by the stress-energy operator, and records the single-particle consistency check together with the application to inflationary perturbations.

I.1 From mass density to stress-energy

The Diósi master equation for point masses is [5, 34]

$$\frac{d\hat{\rho}}{dt} = -\frac{i}{\hbar}[\hat{H},\hat{\rho}] - \frac{G}{2\hbar}\int d^3x\, d^3y\, \frac{[\hat{\mu}(\mathbf{x}),[\hat{\mu}(\mathbf{y}),\hat{\rho}]]}{|\mathbf{x}-\mathbf{y}|}\,, \tag{112}$$

with $\hat{\mu}(\mathbf{x})$ the mass density operator and kernel $1/|\mathbf{x}-\mathbf{y}|$ the Green function of the Poisson constraint $\nabla^2\Phi = 4\pi G\rho$. For a point mass in superposition $(|L\rangle+|R\rangle)/\sqrt{2}$ the double commutator yields $\Gamma = GM^2/(\hbar d)$, recovering the central rate. For quantum fields the mass density generalizes to the energy density divided by c^2, $\hat{\mu} \to \hat{T}^{00}/c^2$, giving the field-theoretic Diósi master equation

$$\boxed{\frac{d\hat{\rho}}{dt} = -\frac{i}{\hbar}[\hat{H},\hat{\rho}] - \frac{G}{2\hbar c^4}\int d^3x\, d^3y\, \frac{[\hat{T}^{00}(\mathbf{x}),[\hat{T}^{00}(\mathbf{y}),\hat{\rho}]]}{|\mathbf{x}-\mathbf{y}|}\,.} \tag{113}$$

For a superposition of two field states with distinct stress-energy expectation values, the off-diagonal element decays as $e^{-\Gamma t}$ with

$$\Gamma = \frac{G}{\hbar c^4}\int d^3x\, d^3y\, \frac{\Delta T^{00}(\mathbf{x})\,\Delta T^{00}(\mathbf{y})}{|\mathbf{x}-\mathbf{y}|}\,, \qquad \Delta T^{00} = \langle\hat{T}^{00}\rangle_1 - \langle\hat{T}^{00}\rangle_2\,, \tag{114}$$

which is the gravitational self-energy of the energy-density difference, divided by $\hbar$. The pointer basis selected by (113) consists of states with definite energy-density distributions: for point particles this is the position basis; for fields it is energy-momentum eigenstates or quasi-classical configurations, not field-amplitude eigenstates.

I.2 Fock-state superpositions and the single-particle limit

For a real massive scalar field in a cubic box of side L, a superposition $(|n\rangle + |m\rangle)/\sqrt{2}$ of two occupation numbers of a single mode $\mathbf{k}$ has a spatially uniform energy-density difference $\Delta T^{00} = (n-m)\hbar\omega_k/V$, with $V = L^3$ and $\omega_k = \sqrt{k^2c^2 + m^2c^4/\hbar^2}$. The vacuum contribution cancels in the difference. Inserting this into (114) and using the geometric double integral over

the cube (Appendix J),

$$\mathcal{J}(L) \equiv \int_{\text{cube}}\int_{\text{cube}} \frac{d^3x\, d^3y}{|\mathbf{x}-\mathbf{y}|} = C_{\text{cube}}\, L^5\,, \qquad C_{\text{cube}} \approx 1.192\,, \tag{115}$$

gives the Fock-state decoherence rate

$$\Gamma_{\text{Fock}} = \frac{G\,(n-m)^2\,\hbar\,\omega_k^2\, C_{\text{cube}}}{c^4\, L}\,. \tag{116}$$

The fundamental prefactor $G\hbar/c^4 \approx 8.7 \times 10^{-79}\,\text{m}^2\,\text{s}$ is extraordinarily small: gravitational decoherence of optical or microwave photon number states gives decoherence times exceeding the age of the universe by tens of orders of magnitude, and is negligible for electromagnetic fields. The rate can become significant only for massive bosons.

A non-trivial consistency check connects (116) to the point-particle result. For a single massive particle ($n = 1$, $m = 0$) in a mode of wavelength $\lambda \sim d$, the frequency is $\omega_k = mc^2/\hbar$ and the mode size is $L \sim d$, so

$$\Gamma = \frac{G\,\hbar\,(mc^2/\hbar)^2\, C_{\text{cube}}}{c^4\, d} = \frac{G\, m^2\, C_{\text{cube}}}{\hbar\, d}\,, \tag{117}$$

which reproduces the Diósi–Penrose rate $GM^2/(\hbar d)$ up to the geometric factor $C_{\text{cube}} \approx 1.192$; in the localized wave-packet limit ($\sigma \ll d$) the self-energy integral reduces to the point-particle result with $C_{\text{cube}} \to 1$. For a multi-mode superposition the rate depends on the *total* energy difference $\Delta E = \sum_k (n_k - m_k)\hbar\omega_k$ as $\Gamma = G(\Delta E)^2 C_{\text{cube}}/(\hbar c^4 L)$, so partially cancelling mode contributions reduce the decoherence while reinforcing ones enhance it.

I.3 Application to inflationary perturbations

Applied to inflation, the same formalism suggests a universal self-gravitational route to the quantum-to-classical transition of primordial perturbations. During slow-roll inflation a scalar mode is squeezed after horizon crossing into a state with mean occupation $\bar{n}_k \approx \frac{1}{4}e^{2N_k}$, where N_k is the number of e-folds since crossing; its gravitational self-energy, evaluated with the Newtonian kernel over a Hubble volume, grows as $E_G(k) \sim (G\hbar^2 H_{\text{inf}}^3/c^5)\, e^{4N_k}/16$. Setting the decoherence rate $\Gamma_k = E_G(k)/\hbar$ equal to the Hubble rate gives

$$N_{\text{dec}} = \frac{1}{4}\ln\!\Big(\frac{16}{\varepsilon_{\text{grav}}}\Big)\,, \qquad \varepsilon_{\text{grav}} \equiv \Big(\frac{\hbar H_{\text{inf}}}{E_P}\Big)^2\,, \tag{118}$$

e-folds after horizon crossing. For GUT-scale inflation ($H_{\text{inf}} \sim 10^{13}$ GeV), $\varepsilon_{\text{grav}} \approx 6.7 \times 10^{-13}$ and $N_{\text{dec}} \approx 7.7$—well before recombination for all observable modes. Physical arguments suggest this provides a universal mechanism for the classicalization of primordial perturbations, with the same parametric dependence on $(H_{\text{inf}}/M_P)^2$ as environmental decoherence but arising from the self-gravitational field alone. The result is a motivated order-of-magnitude estimate subject to $O(1)$ corrections from the de Sitter kernel and gauge choice: the de Sitter propagator differs from the Newtonian kernel only at super-Hubble separations, affecting the coefficient but not the parametric scaling, and the gauge-dependence of T^{00} shifts only the $O(1)$ prefactor. The power spectrum, set by the diagonal density-matrix elements, is unaffected by decoherence, consistent with the success of standard inflationary predictions.

J The Geometric Double Integral

The gravitational self-energy of a uniform density distribution in a cube of side L requires the double integral

$$\mathcal{J}(L) = \int_0^L\!\!\int_0^L\!\!\int_0^L\!\!\int_0^L\!\!\int_0^L\!\!\int_0^L \frac{dx\,dy\,dz\,dx'\,dy'\,dz'}{\sqrt{(x-x')^2+(y-y')^2+(z-z')^2}}\,. \tag{119}$$

By dimensional analysis, $\mathcal{J}(L) = C_{\text{cube}}\,L^5$ for some dimensionless constant C_{cube}.

Convergence. The integrand $1/r$ is integrable in $\mathbb{R}^3$ because the volume element $d^3x\,d^3y$ scales as $r^5\,dr$ near the diagonal $\mathbf{x}=\mathbf{y}$, which overcomes the $1/r$ singularity. The integral is therefore finite without regularization.

Numerical value. The constant has been computed by Chandrasekhar [40] in the context of gravitational self-energy calculations and verified by Ciftja and Wexler [41] using Monte Carlo integration:

$$C_{\text{cube}} = \frac{\mathcal{J}(L)}{L^5} \approx 1.19189\,. \tag{120}$$

For comparison, a uniform sphere of radius R and mass M has the standard self-energy integral $\int\!\int \rho^2/|\mathbf{x}-\mathbf{y}|\,d^3x\,d^3y = \frac{6}{5}\,M^2/R$ (equivalently a gravitational self-energy $U = \frac{1}{2}G\int\!\int \rho^2/r = \frac{3}{5}GM^2/R$), i.e. a coefficient $C_{\text{sphere}} = 6/5 = 1.200$ in the normalization $\int\!\int \rho^2/r = C\,M^2/R$. This is very close to the cube value $C_{\text{cube}} \approx 1.192$ in the same normalization, reflecting the approximate shape-independence of the gravitational self-energy for compact objects.

References

[1] Jacob D. Bekenstein. Black holes and entropy. *Phys. Rev. D*, 7:2333–2346, 1973.

[2] Stephen W. Hawking. Particle creation by black holes. *Commun. Math. Phys.*, 43:199–220, 1975.

[3] Shinsei Ryu and Tadashi Takayanagi. Holographic derivation of entanglement entropy from AdS/CFT. *Phys. Rev. Lett.*, 96:181602, 2006.

[4] Juan Maldacena and Leonard Susskind. Cool horizons for entangled black holes. *Fortschr. Phys.*, 61:781–811, 2013.

[5] Lajos Diósi. A universal master equation for the gravitational violation of quantum mechanics. *Phys. Lett. A*, 120:377–381, 1987.

[6] Roger Penrose. On gravity's role in quantum state reduction. *Gen. Relativ. Gravit.*, 28:581–600, 1996.

[7] Marc Sperzel. Holographic dark energy from information conservation, 2026. Companion paper, Quantum-Geometric Correspondence Series.

[8] Stephen W. Hawking. Breakdown of predictability in gravitational collapse. *Phys. Rev. D*, 14:2460–2473, 1976.

[9] Geoffrey Penington. Entanglement wedge reconstruction and the information paradox. *JHEP*, 09:002, 2020.

[10] Netta Engelhardt and Aron C. Wall. Quantum extremal surfaces: holographic entanglement entropy beyond the classical regime. *JHEP*, 01:073, 2015.

[11] Ahmed Almheiri, Thomas Hartman, Juan Maldacena, Edgar Shaghoulian, and Amirhossein Tajdini. The entropy of Hawking radiation. *Rev. Mod. Phys.*, 93:035002, 2021.

[12] Erik Verlinde. On the origin of gravity and the laws of Newton. *JHEP*, 04:029, 2011.

[13] Joseph J. Bisognano and Eyvind H. Wichmann. On the duality condition for quantum fields. *J. Math. Phys.*, 17:303–321, 1976.

[14] Ted Jacobson. Thermodynamics of spacetime: The Einstein equation of state. *Phys. Rev. Lett.*, 75:1260–1263, 1995.

[15] Gerard 't Hooft. Dimensional reduction in quantum gravity. 1993.

[16] Leonard Susskind. The world as a hologram. *J. Math. Phys.*, 36:6377–6396, 1995.

[17] Raphael Bousso. The holographic principle. *Rev. Mod. Phys.*, 74:825–874, 2002.

[18] Fermi LAT and GBM Collaborations. A limit on the variation of the speed of light arising from quantum gravity effects. *Nature*, 462:331–334, 2009.

[19] Shuang-Nan Zhang et al. Detailed polarization measurements of the prompt emission of five gamma-ray bursts. *Nat. Astron.*, 3:258–264, 2019.

[20] Martin C. Weisskopf et al. The Imaging X-ray Polarimetry Explorer (IXPE): Pre-launch. *J. Astron. Telesc. Instrum. Syst.*, 8:026002, 2022.

[21] Charis Anastopoulos and Bei-Lok Hu. A master equation for gravitational decoherence: probing the textures of spacetime. *Class. Quantum Grav.*, 30:165007, 2013.

[22] Miles Blencowe. Effective field theory approach to gravitationally induced decoherence. *Phys. Rev. Lett.*, 111:021302, 2013.

[23] Richard P. Feynman and Frank L. Vernon Jr. The theory of a general quantum system interacting with a linear dissipative system. *Ann. Phys.*, 24:118–173, 1963.

[24] Amir O. Caldeira and Anthony J. Leggett. Path integral approach to quantum Brownian motion. *Physica A*, 121(3):587–616, 1983.

[25] Bryce S. DeWitt. Quantum theory of gravity. i. the canonical theory. *Phys. Rev.*, 160:1113–1148, 1967.

[26] Roy J. Glauber. Coherent and incoherent states of the radiation field. *Phys. Rev.*, 131:2766–2788, 1963.

[27] Donald Marolf. Refined algebraic quantization in the oscillator representation of $SL(2,\mathbb{R})$. 1995.

[28] Domenico Giulini and Donald Marolf. On the generality of refined algebraic quantization. *Class. Quantum Grav.*, 16:2479–2488, 1999.

[29] Don N. Page and William K. Wootters. Evolution without evolution: Dynamics described by stationary observables. *Phys. Rev. D*, 27:2885–2892, 1983.

[30] Venkatesa Chandrasekaran, Roberto Longo, Geoff Penington, and Edward Witten. An algebra of observables for de Sitter space. *JHEP*, 02:082, 2023.

[31] Edward Witten. Gravity and the crossed product. *JHEP*, 10:008, 2022.

[32] Joseph J. Bisognano and Eyvind H. Wichmann. On the duality condition for a Hermitian scalar field. *J. Math. Phys.*, 16:985–1007, 1975.

[33] Thomas Faulkner, Robert G. Leigh, Onkar Parrikar, and Huajia Wang. Modular Hamiltonians for deformed half-spaces and the averaged null energy condition. *JHEP*, 09:038, 2016.

[34] Lajos Diósi. Models for universal reduction of macroscopic quantum fluctuations. *Phys. Rev. A*, 40:1165–1174, 1989.

[35] Frigyes Károlyházy. Gravitation and quantum mechanics of macroscopic objects. *Nuovo Cim. A*, 42:390–402, 1966.

[36] Charles W. Misner, Kip S. Thorne, and John Archibald Wheeler. *Gravitation*. W. H. Freeman, San Francisco, 1973.

[37] Norman Margolus and Lev B. Levitin. The maximum speed of dynamical evolution. *Physica D*, 120:188–195, 1998.

[38] L. Mandelstam and Ig. Tamm. The uncertainty relation between energy and time in non-relativistic quantum mechanics. *Journal of Physics (USSR)*, 9:249–254, 1945. Reprinted in: *Selected Papers*, Springer (2005).

[39] Seth Lloyd. Ultimate physical limits to computation. *Nature*, 406:1047–1054, 2000.

[40] Subrahmanyan Chandrasekhar. *Ellipsoidal Figures of Equilibrium*. Yale University Press, New Haven, 1969.

[41] Orion Ciftja and Carlos Wexler. A Monte Carlo integration approach to the self-energy of a uniformly charged cube. *J. Math. Phys.*, 46:032110, 2005.